

# The properties of extragalactic radio sources selected at 20 GHz

Elaine M. Sadler,<sup>1</sup> Roberto Ricci,<sup>2</sup> Ronald D. Ekers,<sup>2</sup> J. A. Ekers,<sup>2</sup> Paul J. Hancock,<sup>1</sup>  
 Carole A. Jackson,<sup>2</sup> Michael J. Kesteven,<sup>2</sup> Tara Murphy,<sup>1</sup> Chris Phillips,<sup>2</sup>  
 Robert F. Reinfrank,<sup>3</sup> Lister Staveley-Smith,<sup>2</sup> Ravi Subrahmanyan,<sup>2</sup>  
 Mark A. Walker,<sup>1,2,4</sup> Warwick E. Wilson<sup>2</sup> and Gianfranco De Zotti<sup>5,6</sup>

<sup>1</sup>*School of Physics, University of Sydney, NSW 2006, Australia*

<sup>2</sup>*Australia Telescope National Facility, CSIRO, PO Box 76, Epping, NSW 1710, Australia*

<sup>3</sup>*Department of Physics and Mathematical Physics, University of Adelaide, Adelaide, SA 5005, Australia*

<sup>4</sup>*MAW Technology Pty Ltd, 3/22 Cliff Street, Manly 2095, Australia*

<sup>5</sup>*SISSA/ISAS, Via Beirut 2–4, I-34014 Trieste, Italy*

<sup>6</sup>*INAF, Osservatorio Astronomico di Padova, Vicolo dell'Osservatorio 5, I-35122 Padova, Italy*

Accepted 2006 June 22. Received 2006 June 22; in original form 2006 March 16

## ABSTRACT

We present some first results on the variability, polarization and general properties of radio sources selected at 20 GHz, the highest frequency at which a sensitive radio survey has been carried out over a large area of sky. Sources with flux densities above 100 mJy in the Australia Telescope Compact Array 20 GHz pilot survey at declination  $-60^\circ$  to  $-70^\circ$  were observed at up to three epochs during 2002–04, including near-simultaneous measurements at 5, 8 and 18 GHz in 2003. Of the 173 sources detected, 65 per cent are candidate QSOs or BL Lac objects, 20 per cent galaxies and 15 per cent faint ( $b_J > 22$  mag) optical objects or blank fields.

On a 1–2 yr time-scale, the general level of variability at 20 GHz appears to be low. For the 108 sources with good-quality measurements in both 2003 and 2004, the median variability index at 20 GHz was 6.9 per cent and only five sources varied by more than 30 per cent in flux density.

Most sources in our sample show low levels of linear polarization (typically 1–5 per cent), with a median fractional polarization of 2.3 per cent at 20 GHz. There is a trend for fainter 20 GHz sources to have higher fractional polarization.

At least 40 per cent of sources selected at 20 GHz have strong spectral curvature over the frequency range 1–20 GHz. We use a radio ‘two-colour diagram’ to characterize the radio spectra of our sample, and confirm that the flux densities of radio sources at 20 GHz (which are also the foreground point-source population for cosmic microwave background anisotropy experiments like *Wilkinson Microwave Anisotropy Probe* and *Planck*) cannot be reliably predicted by extrapolating from surveys at lower frequencies. As a result, direct selection at 20 GHz appears to be a more efficient way of identifying 90 GHz phase calibrators for Atacama Large Millimeter Array (ALMA) than the currently proposed technique of extrapolation from radio surveys at 1–5 GHz.

**Key words:** surveys – galaxies: active – cosmic microwave background – radio continuum: galaxies – radio continuum: general.

## 1 INTRODUCTION

Most large-area radio imaging surveys have been carried out at frequencies of 1.4 GHz or below, where the long-term variability of the radio-source population is generally low. The catalogued flux densities measured by such surveys can therefore continue to be

used with a high level of confidence for many years after the survey was made.

It is not clear to what extent this is true for radio surveys carried out at higher frequencies, where the source population becomes increasingly dominated by compact, flat-spectrum sources which may be variable on time-scales of a few years.

We are currently carrying out a sensitive radio survey of the entire southern sky at 20 GHz, using a wide-band analogue correlator on the Australia Telescope Compact Array (ATCA; see Ricci et al.

\*E-mail: ems@physics.usyd.edu.au

2004a, for an outline of the pilot study for this survey). We have therefore begun an investigation of the long-term variability of radio sources selected at 20 GHz, which will also help us estimate the likely long-term stability of our source catalogue.

There is little information to guide us in what to expect. Only a few studies of radio-source variability have been carried out at frequencies above 5 GHz and these have generally targeted sources which were either known to be variable at lower frequencies, or were selected to have flat or rising radio spectra at frequencies below about 5 GHz. Such objects may not be typical of the 20 GHz source population as a whole.

The full AT 20 GHz (AT20G) survey, using the whole 8 GHz bandwidth of the analogue correlator and coherently combining all three interferometer baselines, began in late 2004 and has a detection limit of 40–50 mJy at 20 GHz, i.e. about a factor of 2 fainter than the sources discussed here. It will eventually cover the entire southern sky from declination Dec.  $0^\circ$  to  $-90^\circ$ .

Our reasons for carrying out a pilot survey in advance of the full AT20G survey were to characterize the high-frequency radio-source population, and to optimize the observational techniques used in the two-step survey process (i.e. fast scans of large areas of sky with a wide-band analogue correlator, followed by snapshot imaging of candidate detections) to maximize the completeness, reliability and uniformity of the final AT20G catalogue. Because of the slightly different observational techniques used in 2002, 2003 and 2004, the pilot survey data are not as complete or uniform as the AT20G data are intended to be. The pilot survey nevertheless provides an important first look at the faint radio-source population at 20 GHz. Since corrections for extragalactic foreground confusion will be critical for next-generation cosmic microwave background (CMB) surveys, a better knowledge of the properties of high-frequency radio sources (and especially their polarization and variability) is particularly desirable.

This paper presents an analysis of the radio-source population down to a limiting flux density of about 100 mJy at 20 GHz, based on observations in the Dec. zone  $-60^\circ$  to  $-70^\circ$  scanned by the AT 20 GHz pilot survey in 2002 and 2003. Our aim is to provide some first answers to the following questions.

(i) How does the radio-source population at 20 GHz relate to the ‘flat-spectrum’ and ‘steep-spectrum’ populations identified at lower frequencies?

(ii) What fraction of radio sources selected at 20 GHz are variable on time-scales of a few years, and how stable in time is a 20 GHz source catalogue?

(iii) What are the polarization properties of radio continuum sources selected at 20 GHz?

## 2 OBSERVATIONS

### 2.1 The ATCA wide-band correlator

An analogue correlator with 8 GHz bandwidth (Roberts, Leach & Wilson, in preparation), originally developed for the Taiwanese CMB instrument AMiBA (Lo et al. 2001) is currently being used at the ATCA to carry out a radio continuum survey of the entire southern sky at 20 GHz. The wide bandwidth of this correlator, combined with the fast scanning speed of the ATCA, makes it possible to scan large areas of sky at high sensitivity despite the small (2.3 arcmin) field of view at 20 GHz. Since delay tracking cannot be performed with this wide-band analogue correlator, all scanning observations are carried out on the meridian (where the delay for an east–west interferometer is zero).

The fast-scanning survey measures approximate positions and flux densities for all candidate sources above the detection threshold of the survey. Follow-up 20 GHz imaging of these candidate detections is then carried out a few weeks later, using the ATCA in a hybrid configuration with its standard (delay-tracking) digital correlator. These follow-up images allow us to confirm detections, and to measure accurate positions and flux densities for the detected sources. Finally, the confirmed sources are also imaged at 5 and 8 GHz to measure their radio spectra, polarization and angular size.

### 2.2 Observations in the $-60^\circ$ to $-70^\circ$ Dec. zone

Tables 1 and 2 summarize the telescope and correlator configurations used for the observations discussed in this paper. There are three main data sets.

(i) The ATCA pilot survey observations made in 2002 and published by Ricci et al. (2004a). These are briefly described in Section 2.4 below.

(ii) Data from a resurvey of the same Dec. zone at 20 GHz in 2003, together with near-simultaneous observations at 4.8 and 8.6 GHz of the confirmed sources (see Section 2.5).

(iii) 20 GHz images made in 2004 of sources detected at 18 GHz in 2002 and/or 2003, as part of a program to monitor the long-term variability of the sources detected in the pilot survey (Section 2.6).

Although our ATCA 20 GHz pilot survey covered the whole sky between Dec.  $-60^\circ$  and  $-70^\circ$ , only sources with Galactic latitude  $|b| > 10^\circ$  are discussed in this paper. While the source population at  $2 < |b| < 10^\circ$  is also dominated by extragalactic objects, it is very difficult to make optical identifications of radio sources close to the Galactic plane because of the high density of foreground stars. Since one aim of this study is to examine the optical properties of high-frequency radio sources, we therefore chose to exclude the small number of extragalactic sources which lay within  $10^\circ$  of the Galactic plane, or within 5:5 of the centre of the Large Magellanic Cloud (LMC).

**Table 1.** log of ATCA fast-scanning observations with the wide-band analogue correlator in the Dec. zone  $-60^\circ$  to  $-70^\circ$ .  $N_{\text{ant}}$  is the number of antennas used for each scanning session.

Date	$N_{\text{ant}}$	$\nu_{\text{cen}}$ (GHz)	Bandwidth (GHz)	Baselines (m)
2002 September 13–17	2	18	3.4	30
2003 October 9–16	3	17.6, 20.4	6–7	30, 30, 60

**Table 2.** log of follow-up ATCA imaging observations of sources detected in the scanning survey at 20 GHz.  $N_{\text{ant}}$  shows the number of antennas equipped with 12 mm receivers for each observing session. The angular resolution of the follow-up images is typically 8 arcsec at 4.8 GHz, 4 arcsec at 8.6 GHz and 15 arcsec at 20 GHz.

Date	ATCA configuration	Observed frequency (GHz)	$N_{\text{ant}}$
2002 October 8–12	H168B	17.2, 18.8	3
2003 November 3–6	H214	17.0, 19.0, 21.0, 23.0	5
2003 November 8–10	1.5D	4.8, 8.6	5
2004 October 21–28	H214	19.0, 21.0	5

### 2.3 The flux-density scale of the ATCA at 20 GHz

At centimetre wavelengths, the ATCA primary flux calibrator is the radio galaxy PKS1934–638 (Reynolds 1994). Planets have traditionally been used to set the flux-density scale in the 12 mm (18–25 GHz) band, and the planets Mars and Jupiter were used as primary flux calibrators during the first two years of operation of the ATCA 12-mm receivers in 2002–03. However, the use of planets to set the flux-density scale has some significant disadvantages (Sault 2003) as discussed in the following.

(i) Their angular size (4–25 arcsec for Mars and 30–48 arcsec for Jupiter) means that they can be resolved out at 20 GHz on baselines greater than a few hundred metres.

(ii) Their (northern) location on the ecliptic means that they are visible above the horizon for a much shorter time than a southern source like PKS1934–38, and shadowing of northern sources can also be a problem in some compact ATCA configurations.

PKS1934–638 was monitored regularly in the 12 mm band over a six-month period in 2003, using Mars as primary flux calibrator (Sault 2003). These observations showed that the flux density of PKS1934–638 remained constant (varying by less than  $\pm 1$  to 2 per cent at 20 GHz), making it suitable for use as a flux calibrator at these high frequencies. From 2004, therefore, PKS1934–638 was used as the primary flux ATCA calibrator at 20 GHz, whereas Mars was used in our 2002 and 2003 observations.

### 2.4 2002 observations

#### 2.4.1 Scanning observations

The first observations of the Dec. strip  $-60^\circ$  to  $-70^\circ$  were made by Ricci et al. (2004a). Using a single analogue correlator with 3 GHz bandwidth and two ATCA antennas on a single 30 m baseline, they detected 123 extragalactic ( $|b| > 5^\circ$ ) sources at 18 GHz above a limiting flux density of 100 mJy. The 2002 observations did not completely cover the whole  $-60^\circ$  to  $-70^\circ$  Dec. strip because of technical problems which interrupted some of the fast scanning runs. Fig. 4 of Ricci et al. (2004a) shows the 2002 sky coverage and the missing regions, which are mainly in the right ascension (RA) range 5–8 h. The Dec.  $-60^\circ$  to  $-70^\circ$  strip was therefore re-observed at 22 GHz in 2003, and full coverage was then achieved. The region overlapped by the 2002 and 2003 observations gives a useful test of the completeness of the scanning survey technique, as discussed in Section 4.

#### 2.4.2 Follow-up imaging and flux-density errors

Follow-up synthesis imaging of the candidate sources detected in the 2002 scans was carried out at 18 GHz with the ATCA as described by Ricci et al. (2004a). It is important to note that, because the candidate source positions obtained from the wide-band scans in 2002 were typically accurate to  $\sim 1$  arcmin, and the primary beam of the ATCA antennas at 20 GHz is only  $\sim 2.3$  arcmin, about 30 per cent of the sources detected in the follow-up images were offset by 80 arcsec or more from the pointing centre, and so required large (more than a factor of 2) corrections to their observed flux densities to correct for the attenuation of the primary beam. These corrections were made by Ricci et al. (2004a), but were not explicitly discussed in their paper. It has subsequently become clear that uncertainties in the primary beam correction at very large offsets from the field centre can sometimes introduce large systematic errors into

the observed fluxes. For this reason, we now regard the 18 GHz flux-density measurements listed by Ricci et al. (2004a) as unreliable for sources observed at more than 80 arcsec from the imaging field centre. For follow-up imaging in 2003 and subsequent years, sources more than 80 arcsec from the imaging field centre were re-observed at the correct position whenever possible.

### 2.5 2003 observations

#### 2.5.1 Scanning observations

In 2003, we used three analogue correlators and three ATCA antennas, giving us three independent baselines (of 30, 30 and 60 m). The correlators also had a new design with the potential for 8 GHz operation (Roberts et al. in preparation). The 2003 fast scans were carried out using three ATCA antennas separated by 30 m on an east–west baseline, and scanned in a trellis pattern at  $15 \text{ deg min}^{-1}$  with  $11^\circ$  scans from Dec.  $-59:5$  to  $-70:5$ , interleaved with 2.3 arcmin separation and sampled at 54 ms.

The system temperature was continually monitored at 17.6 and 20.4 GHz and periods with high sky noise (i.e. due to clouds or rain) were flagged out and repeated later. Calibration sources were observed approximately once per day by tracking them through transit ( $\pm 5$  min).

Due to an unforeseen problem matching the wide-band receiver output to the fibre modulator, there was a 15 db slope across the bandpass. When we transformed the 16 lag channels observed into eight complex frequency channels, the resulting bandpass was uncalibratable and unphysical. This occurred because we had an analogue correlator and there is no exact Fourier transform relation between delay and frequency (Harris & Zmuidzinas 2001).

The actual bandpass was measured by taking the Fourier transform of the time sequence obtained while tracking a calibrator source through transit. In this case, we have a physical delay which changes as the earth rotates and we can get a sensible bandpass. In the end only two channels were usable, giving a total band width of 3 GHz. It was also impractical to make a phase calibration of the three interferometers with this data. As a result the sensitivity in 2003 was only marginally better than that in 2002, and overlapping scans could not be combined coherently.

To extract a candidate source list from the 2003 raster scans, the correlator delays were cross-matched with the template delay pattern of a strong calibrator. The correlator coefficient for each time stamp along the scans was recorded, and values from overlapping scans were incoherently combined to form images in 12 equal-area zenithal projection maps (each  $2^h$  wide in RA). The source finding algorithm *imsad* implemented in MIRIAD was used to extract candidate sources above a  $5\sigma$  threshold.

#### 2.5.2 Follow-up imaging

A list of 1350 candidate sources detected in the scanning survey was observed at 17, 19, 21 and 23 GHz as noted in Table 2. As in 2002, the planet Mars was used as the primary flux calibrator. In the 2003 follow-up imaging, the data were reduced as the observations progressed, and sources which were more than 80 arcsec from the imaging centre were re-observed if possible. This significantly improved the accuracy of the flux-density measurements for the 2003 images compared to those made in 2002, as can be seen in Fig. 1.

Images of each follow-up field were made at 18 and 22 GHz using the multifrequency synthesis (MFS) technique. (Conway, Cornwell

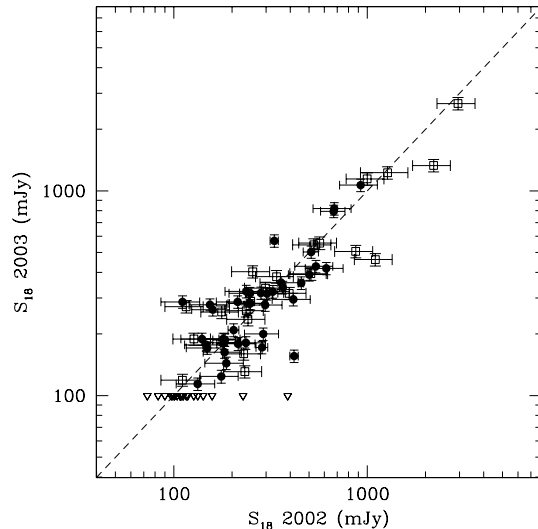


**Figure 1.** Comparison of the 18 GHz flux densities measured in 2002 and 2003 for sources detected independently in the scanning process. Sources which were detected in 2002 but not recovered in 2003 are shown as open triangles with a flux-density limit of 100 mJy for 2003. As discussed in the text, the error bars on the 2002 flux-density measurements are significantly larger than for 2003. Open squares show sources with offsets of more than 80 arcsec from the imaging field centre in the 2002 data.

& Wilkinson 1990; Sault & Wieringa 1994). Since the signal-to-noise ratio (S/N) in the 18 GHz band was significantly higher than at 22 GHz, we used only the 18 GHz data in our subsequent analysis. The median rms noise in the follow-up images was  $1.5 \text{ mJy beam}^{-1}$  at 18 GHz, and sources stronger than five times the rms noise level (estimated from the V-Stokes images) were considered to be genuine detections. The 364 sources with confirmed detections at 18 GHz (including some Galactic plane sources) were imaged at 5 and 8.6 GHz in 2003 November. The total integration time for these follow-up images was 80 s (two cuts) at 17–19 and 21–23 GHz, and 180 s (six cuts) at 5 and 8 GHz.

## 2.6 2004 observations

A sample of 200 sources detected at 18 GHz in 2002 and/or 2003 was re-imaged on 2004 October 22 in a series of targeted observations at 19 and 21 GHz, using the ATCA hybrid configuration H214. All these imaging observations were centred at the source position measured in 2002/2003, so that positional offsets from the imaging field centre were negligible. The 19 and 21 GHz data were combined to produce a single 20 GHz image of each target source. The total integration time at 20 GHz was 240 s (two cuts), and the median rms noise in the final images was 0.7 mJy.

## 3 DATA REDUCTION AND SOURCE FITTING

### 3.1 Reduction of the follow-up images

For the 2003 data, deconvolved images of the confirmed sources were made at 5, 8 and 18 GHz and positions and peak flux densities were measured using the MIRIAD task `maxfit`, which is optimum for a point source. We also used the MIRIAD task `imfit` to measure the integrated flux density and angular extent of extended sources. Where necessary, the fitted flux densities were then corrected for the primary beam attenuation at frequencies between 17 and

23 GHz based on a polynomial model of the Compact Array antenna pattern.

Positional errors were estimated by quadratically adding a systematic term and a noise term: the systematic term was assessed by cross-matching the 18 GHz source positions with the Ma et al. (1998) International Coordinate Reference Frame source positions; the noise term is calculated from the synthesized beam size divided by the flux S/N. The median position errors are  $1''.3$  in RA and  $0''.6$  in Dec.

To estimate the flux-density errors, we quadratically added the rms noise from V-Stokes images to a multiplicative gain error estimated from the scatter between snapshot observations of the strongest sources. The median percentage gain errors were 2 per cent at 5 and 8 GHz, and 5 per cent at 18 GHz.

For the 2004 data, the 19 and 21 GHz visibilities were amplitude and phase calibrated in MIRIAD. As noted in Section 2.3, PKS B1934–638 was used as the primary flux calibrator. The calibrated visibilities were combined to form 20 GHz images using the MFS technique and peak fluxes were worked out using the MIRIAD task `maxfit`. Position and flux errors were determined in the same way as for the 2003 data (see Fig. 2).

### 3.2 Polarization measurements

As all four Stokes parameters were available, linear polarization measurements were carried out on the 2003 and 2004 data. Q-Stokes, U-Stokes and polarized flux  $P = \sqrt{(Q^2 + U^2)}$  were calculated at the peak of the total intensity emission at 20 GHz. The rms in the V-Stokes image for each source was used as an estimate of the noise in U and Q. This error estimate is then used to correct to first order for the Rician bias in P (Leahy 1989) and to set the  $3\sigma$  lower limit on P. Note that this estimate corresponds to the integrated polarization for unresolved sources but is only the polarization at the peak in I for resolved sources. Since over 95 per cent of the sources in our sample are unresolved at 20 GHz (see Section 3.4), this is not a serious problem.

Although the measurements of fractional linear polarization made in 2003 and 2004 were in good general agreement, the 2004 measurements had lower error bars and detected fractional polarizations as low as 1–2 per cent, whereas the 2003 measurements detected only the most highly polarized sources with typical fractional polarizations of 4–5 per cent or higher. We therefore use only the 2004 data in the analysis in Section 8.2 of this paper. A more detailed analysis of extended sources, and of the linear polarized flux and position angle (PA) at 5, 8 and 20 GHz will be presented in a later paper.

Fig. 3 compares our measurements of fractional linear polarization with those made by Ricci et al. (2004b) at 18.5 GHz for objects in common. We find a systematic difference of about 1 per cent in the two data sets, and have investigated this in consultation with authors of the Ricci et al. (2004b) paper. We find that the Ricci et al. (2004b) polarization values are about 1 per cent too high because these observers used a triple correlation method to measure polarized flux (poor phase stability during their run meant that they were not able to produce calibrated images) and did not remove the polarization bias from their data. We estimate that the polarization bias in the Ricci et al. (2004b) data contributes roughly 10 mJy of spurious flux to their polarization measurements. Since their sources have typical 18 GHz flux densities of  $\sim 1 \text{ Jy}$ , this corresponds to a  $\sim 1$  per cent increase in the measured fractional polarization compared to the true value.

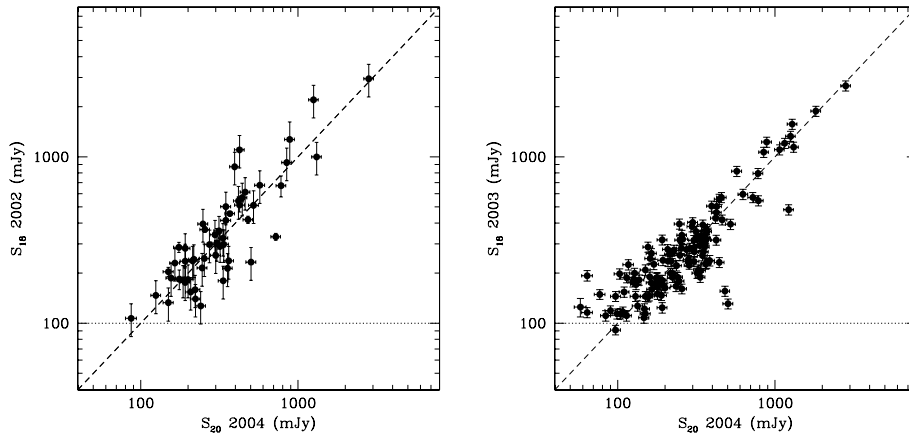


**Figure 2.** Comparison of 18 GHz flux densities measured in 2002 and 2003 with 20 GHz flux densities measured in 2004. The horizontal dotted line shows the sensitivity limit of the 2002 and 2003 surveys.

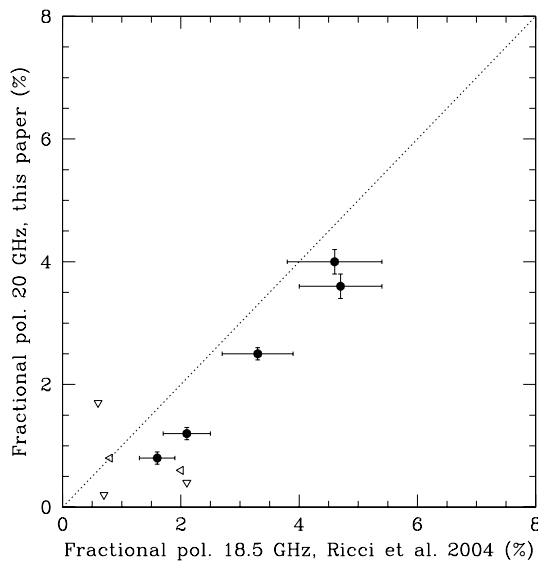


**Figure 3.** Comparison of the fractional linear polarization measured at 20 GHz in this paper with the value measured at 18.5 GHz by Ricci et al. (2004b) for sources in common. Filled circles show objects with polarization detected in both studies, and open triangles show upper limits.

### 3.3 The combined 20 GHz sample 2002–04

Table 3 presents the observed flux densities (in mJy) for extragalactic sources with flux densities above 100 mJy at 20 GHz. As noted in Section 2.2, sources which have low Galactic latitude ( $|b| < 10^\circ$ ), or lie within  $5:5$  of the centre of the LMC, have been excluded. A few sources with measured flux densities consistently less than 100 mJy in the follow-up images were also omitted from the table. These sources are below the detection limit of the scanning survey and were found by chance in the follow-up images, which cover a much smaller area of sky but reach a detection limit of a few mJy at 20 GHz.

The columns in Table 3 are as follows.

- (1) The AT source name, followed by # if the source is resolved or double at 20 GHz (see Section 3.4).
- (2) The radio position (J2000.0) measured from the 20 GHz images. For resolved doubles, the listed position is the radio centroid.

- (3) For sources where we were able to make an optical identification on the Digitized Sky Survey (DSS), this column lists the  $b_j$  magnitude from the SuperCOSMOS data base.

- (4) The object type of the optical ID, as classified in SuperCOSMOS:  $T = 1$  for a galaxy,  $T = 2$  for a stellar object (QSO candidate).  $T = 0$  indicates either a blank field at the source position or a faint ( $>22$  mag) object for which the SuperCOSMOS star/galaxy separation is unreliable.

- (5) The 18 GHz flux density measured in 2002, followed by its error. For resolved doubles, we list the integrated flux density over the source. Flux densities in square brackets [] are measurements made at offsets of more than 80 arcsec from the imaging field centre at 18–20 GHz, and should be regarded as unreliable because of the large primary-beam correction. Flux densities followed by a colon are measured at offsets of 60–80 arcsec from the field centre, but should be reliable.

- (7) The 18 GHz flux density measured in 2003, and its error.

- (9) The 20 GHz flux density measured in 2004, and its error.

- (11) The 8.6 GHz flux density measured in 2003, and its error.

- (13) The 4.8 GHz flux density measured in 2003, and its error.

- (15) The integrated flux density at 843 MHz and its error, from the Sydney University Molonglo Sky Survey (SUMSS) catalogue (Mauch et al. 2003).

- (17) The fractional linear polarization at 20 GHz measured in 2004, and its error.

- (19) The debiased variability index at 20 GHz, calculated as described in Section 5.1.

- (20) Alternative source name, from the NASA/IPAC Extragalactic Database (NED).

- (21) Notes on individual sources, coded as follows:

- C = listed in the online ATCA calibrator catalogue,
- E = possible EGRET gamma-ray source (Tornikoski et al. 2002),
- I = listed as an IRAS galaxy in the online NED,
- M = galaxy detected in the near-infrared two-Micron All-Sky Survey,
- P = in the Parkes quarter-Jy sample (Jackson et al. 2002),
- Q = listed as a QSO in NED,
- V = VLBI observation with the VSOP satellite (Hirabayashi et al. 2000),
- W = source detected in the first-year *Wilkinson Microwave Anisotropy Probe* (WMAP) data (Bennett et al. 2003),
- X = listed as an X-ray source in NED,
- \* = polarization observation by Ricci et al. (2004b).

**Table 3.** Radio spectra and optical IDs for extragalactic 18 GHz sources ( $b > 10^\circ$ , and excluding objects within  $5''.5$  of the LMC centre). Sources marked with # in column 1 are resolved doubles in our 18–20 GHz images; for these objects, the position is that of the radio centroid and the flux density is the total for both components.

(1) Name	(2) Radio position (J2000)	(3) $B$ (mag)	(4) $T$	(5) $S_{18}$ 2002	(6) $S_{18}$ ±	(7) $S_{18}$ 2003	(8) $S_{20}$ ±	(9) $S_{20}$ 2004	(10) $S_8$ ±	(11) $S_8$ 2003	(12) $S_5$ ±	(13) $S_5$ 2003	(14) $S_{843}$ ±	(15) $S_{SUMSS}$ ±	(16) Polarization ±	(17) Polarization (per cent)	(18) ±	(19) Variability (per cent)	(20) Alternate name	(21) Notes
0007–6113	00 07 20.85	-61 13 06.8	19.92	2	-	145	10	150	8	142	3	143	3	87	3	<2.3	-	<6.0	PMNJ0007–6112	
0024–6820	00 24 06.98	-68 20 54.4	17.62	2	366	14	338	24	256	13	388	8	471	9	1250	38	1.7	0.3	PKS0021–686	MX
0025–6028#	00 25 15.91	-60 28 27.6	>22	0	94	19	-	92	5	-	-	-	-	-	1777	69	<7.6	-	PKS0022–60	
0103–6439	01 03 33.93	-64 39 08.0	18.88	1	290	58	200	14	333	19	215	9	173	5	770	69	<1.0	-	PKS0101–649	M
0109–6049	01 09 15.61	-60 49 48.9	22.01	1	[872]	194	506	35	396	20	699	13	787	14	481	15	0.6	0.2	PKS0107–610	CQ
0110–6315	01 10 16.87	-63 15 56.3	20.12	2	154	34	278	19	208	10	165	3	155	3	178	5	<1.4	-	PKS0108–635	QP
0112–6634	01 12 19.05	-66 34 45.3	17.86	2	415	92	295	21	348	17	413	8	474	16	451	49	3.0	0.2	PKS0110–668	QP
0113–6753	01 13 11.50	-67 53 03.2	20.86	2	[127]	28	189	13	241	12	112	3	108	2	68	2	2.7	0.4	PMNJ0113–6753	
0121–6309#	01 21 40.64	-63 09 02.9	17.63	2	-	[121]	8	71	4	293	9	418	9	2650	97	<7.9	-	PKS0119–63	QX $z = 0.837$	
0144–6421	01 44 16.89	-64 21 42.9	21.35	2	286	20	172	12	175	9	201	4	188	3	108	3	4.8	0.6	PMNJ0144–6421	
0154–6604	01 54 31.57	-66 04 16.4	18.87	2	-	245	17	161	8	296	6	390	7	954	29	4.3	0.5	PKS0153–663	QP	
0158–6411	01 58 37.00	-64 11 28.4	19.51	1	133	30	114	8	150	8	132	3	132	2	191	6	4.4	0.6	PMNJ0158–6411	
0158–6334	01 58 55.11	-63 34 49.7	19.29	2	[111]	25	119	8	90	5	144	3	192	4	559	17	7.0	0.8	PKS0157–638	
0201–6638	02 01 07.76	-66 38 12.9	20.26	2	-	207	14	337	17	246	5	270	5	168	5	2.7	0.2	PMNJ0201–6638		
0206–6143	02 06 40.01	-61 43 32.4	20.01	2	-	236	17	209	11	205	4	211	4	220	7	3.7	0.2	PMNJ0206–6143		
0207–6837	02 07 50.94	-68 37 55.0	20.15	2	-	244	17	-	300	6	332	6	400	12	-	-	-	-	PKS0206–688	QP
0208–6216	02 08 01.18	-62 16 35.6	18.24	2	158	35	-	151	8	-	-	-	-	193	6	<1.5	-	PMNJ0207–6216		
0214–7027	02 14 04.60	-70 27 06.3	19.35	2	[149]	33	-	385	19	-	-	-	-	108	3	1.0	0.2	PMNJ0214–7027		
0214–6149	02 14 16.25	-61 49 33.8	20.33	2	248	55	316	22	423	21	220	4	217	4	212	7	2.0	0.1	PKS0212–620	
0219–6806	02 19 41.77	-68 06 18.2	20.08	1	-	226	16	170	9	221	4	279	5	729	22	1.3	0.4	PKS0218–683	P	
0220–6330	02 20 54.20	-63 30 19.6	19.11	2	-	367	26	367	18	333	6	363	7	368	11	2.0	0.2	PKS0219–637	QP	
0230–6214	02 30 11.60	-62 14 35.5	19.20	2	-	146	10	159	8	85	2	93	2	100	3	<1.0	-	PMNJ0230–6214		
0236–6136	02 36 53.25	-61 36 15.1	18.18	2	[511]	113	394	28	522	26	338	7	338	6	604	18	4.4	0.1	PKS0235–618	CQXP
0247–6325	02 47 11.06	-63 25 38.3	17.87	1	-	154	11	110	6	80	2	44	1	12	1	<1.8	-	15.9		M
0250–6355	02 50 36.23	-63 55 01.6	19.67	2	-	147	10	190	10	162	3	158	3	109	3	4.2	0.3	PMNJ0250–6355		
0251–6000	02 51 26.27	-60 00 06.3	19.78	2	-	286	20	308	15	395	8	402	7	274	8	8.6	0.2	PKS0250–602	QP	
0257–6112#	02 57 36.36	-61 12 30.4	18.78	2	-	79	8	101	5	128	4	150	4	382	12	<2.3	-	PKS0256–614		
0303–6458	03 03 50.57	-64 58 54.5	>22	0	149	33	171	12	131	7	156	3	146	3	48	2	<1.5	-	PMNJ0303–6458	P
0303–6211	03 03 50.67	-62 11 25.2	19.48	2	[2202]	489	1330	93	1256	63	1941	37	2181	40	2513	75	2.5	0.1	PKS0302–623	CQXWV*
0304–7007	03 04 18.26	-70 07 41.4	19.09	2	-	190	13	160	8	271	5	311	6	238	7	3.7	0.4	PKS0304–703		
0309–6058	03 09 56.13	-60 58 38.9	19.00	2	-	1207	84	1152	58	1244	24	1348	24	993	30	0.8	0.1	PKS0308–611	CQWV*	
0314–6548	03 14 22.44	-65 48 24.7	19.06	2	297	66	277	19	274	14	164	3	161	3	354	11	3.0	0.2	PKS0313–660	QX $z = 0.636$
0323–6026	03 23 08.44	-60 26 31.3	20.69	2	159	35	263	18	222	11	220	4	223	4	199	6	2.2	0.2	PMNJ0323–6026	
0340–6811	03 40 06.53	-68 11 26.1	22.01	1	-	200	14	128	6	207	10	160	3	225	7	3.7	0.5	PKS0339–683		
0340–6703	03 40 28.27	-67 03 16.6	19.24	2	[177]	39	256	18	249	12	222	4	210	4	374	11	<0.8	-	PMNJ0340–6703	P
0341–5954	03 41 21.60	-59 54 08.6	18.21	2	147	33	177	12	125	6	195	4	212	4	379	11	<2.0	-	PKS0340–600	
0355–6645	03 55 47.86	-66 45 33.9	19.00	2	-	293	21	334	17	483	9	581	11	1403	42	1.6	0.2	PKS0355–66	CQP	
0357–6948	03 57 30.07	-69 48 45.6	>22	0	[231]	51	-	111	6	-	-	-	-	148	5	<1.9	-	PMNJ0357–6948		
0408–6545	04 08 20.33	-65 45 08.7	>22	0	543	121	428	30	419	21	1540	30	3188	58	25029	751	3.6	0.2	PKS0408–65	C*
0420–6223	04 20 56.09	-62 23 38.6	>22	0	-	188	13	179	9	482	9	896	16	5622	169	2.1	0.3	PKS0420–62	C	

**Table 3 – continued**

(1) Name	(2) Radio position (J2000)	(3) B (mag)	(4) T	(5) S <sub>18</sub> 2002	(6) S <sub>18</sub> 2003	(7) S <sub>18</sub> 2003	(8) S <sub>20</sub> 2004	(9) S <sub>20</sub> 2004	(10) S <sub>8</sub> 2003	(11) S <sub>8</sub> 2003	(12) S <sub>5</sub> 2003	(13) S <sub>5</sub> 2003	(14) S <sub>843</sub> SUMSS	(15) S <sub>843</sub> SUMSS	(16) ±	(17) Polarization (per cent)	(18) ±	(19) Variability (per cent)	(20) Alternate name	(21) Notes
0421–6729	04 21 19.71	–67 29 01.6	20.16	1	–	–	127	9	134	10	124	3	79	2	39	2	<1.4	–	<6.0	
0422–6507	04 22 29.15	–65 07 05.0	20.42	2	[108]	24	–	–	103	5	–	–	–	–	177	6	2.1	0.6	–	PMNJ0422–6507
0425–6646	04 25 06.77	–66 46 49.8	20.59	2	[242]	54	236	17	218	11	315	6	361	7	91	3	2.4	0.3	<6.0	PKS0425–669
0428–6438	04 28 10.87	–64 38 22.6	21.63	1	180	40	189	13	335	17	168	3	140	3	78	3	<0.7	–	27.4	PMNJ0428–6438
0433–6030	04 33 34.08	–60 30 13.1	19.10	1	359	80	356	25	315	16	324	6	325	6	414	13	2.0	0.2	<6.0	PKS0432–606
0436–6056	04 36 21.77	–60 56 37.3	21.85	2	–	–	[491]	44	116	6	–	–	–	–	136	4	3.7	0.6	–	
0436–5931	04 36 51.52	–59 31 36.6	15.53	1	–	–	149	10	77	4	114	2	125	2	96	3	<2.3	–	–	ESO118–IG32
0449–6106	04 49 24.33	–61 06 26.4	>22	0	–	–	172	12	192	10	237	5	256	5	427	13	3.9	0.3	<6.0	PKS0448–611
0504–6049	05 04 01.65	–60 49 52.5	19.43	2	[116]	26	[272]	19	168	8	–	–	–	–	568	17	<1.2	–	–	PKS0503–608
0505–6215	05 05 46.75	–62 15 44.8	19.42	2	157	35	[287]	20	86	5	–	–	–	–	54	2	<2.1	–	–	PMNJ0505–6215
0505–6236	05 05 48.53	–62 36 11.0	20.80	2	152	34	[201]	16	87	5	–	–	–	–	110	3	2.9	0.7	–	PMNJ0505–6236
0506–6109	05 06 43.96	–61 09 41.0	17.16	2	–	–	1883	131	1819	91	1756	34	1791	33	3102	93	1.2	0.1	<6.0	PKS0506–61
0507–6107	05 07 54.62	–61 04 43.2	21.18	2	–	–	232	16	443	22	336	7	420	8	842	25	0.6	0.2	30.8	MRC0507–611
0516–6204	05 16 44.89	–62 07 05.4	21.20	2	[530]	118	545	38	785	39	414	8	416	8	418	13	2.8	0.1	–	PKS0516–621
0522–6107	05 22 34.39	–61 07 57.2	18.46	2	[1101]	244	462	32	425	21	654	13	700	13	741	22	0.8	0.2	<6.0	PKS0522–611
0534–6106	05 34 35.73	–61 06 07.0	19.29	1	513	47	503	35	426	30	435	8	491	9	451	14	1.6	0.2	6.6	PKS0534–611
0546–6415	05 46 41.83	–64 15 22.1	16.54	2	–	–	227	16	363	21	189	4	243	4	119	4	<0.6	–	22.5	PMNJ0546–6415
0607–6031	06 07 55.13	–60 31 52.0	19.50	2	–	–	161	11	256	13	286	6	406	7	1416	43	1.7	0.2	26.1	PKS0607–605
0610–6058	06 10 30.36	–60 58 37.8	20.15	2	–	–	145	10	130	7	186	4	215	4	350	11	2.9	0.4	–	PKS0609–609
0620–6107	06 20 05.24	–61 07 31.6	19.99	2	–	–	167	12	235	12	255	5	287	5	357	11	10.0	0.3	16.1	
0621–5935	06 21 53.13	–59 35 08.6	19.68	1	–	–	222	16	237	12	396	8	547	10	1276	38	0.8	0.2	<6.0	PKS0621–595
0623–6436	06 23 07.75	–64 36 20.7	17.06	1	–	–	481	34	1222	61	368	7	312	6	326	13	0.5	0.1	43.2	PMNJ0623–6436
0625–6020	06 25 24.32	–60 20 29.8	>22	0	–	–	269	19	351	18	342	7	365	7	288	9	<0.6	–	12.2	PMNJ0625–6020
0628–6248	06 28 57.54	–62 48 45.0	21.24	2	–	–	327	23	359	18	396	8	426	8	522	16	7.1	0.2	<6.0	PKS0628–627
0644–6712	06 44 28.15	–67 12 57.6	21.53	1	–	–	230	16	368	18	225	4	233	4	218	7	6.6	0.2	22.5	PKS0644–671
0647–6058	06 47 40.86	–60 58 05.3	>22	0	–	–	145	10	97	5	93	2	98	2	108	3	2.4	0.5	–	PMNJ0647–6058
0650–6510	06 50 57.62	–65 10 12.3	18.69	2	–	–	91	6	97	5	174	3	207	4	71	2	3.6	0.6	<6.0	PMNJ0650–6509
0700–6610	07 00 31.16	–66 10 45.2	15.77	2	–	–	235	16	306	15	293	6	298	5	288	9	3.0	0.2	12.1	PKS0700–661
0715–6829	07 15 09.51	–68 29 58.2	–	–	–	–	209	15	327	16	236	5	239	4	143	4	6.0	0.2	21.4	PMNJ0715–6829
0716–6240	07 16 33.57	–62 40 26.5	20.27	2	–	–	316	22	364	18	226	4	182	3	116	4	2.7	0.2	<6.0	PKS0716–625
0719–6218	07 19 04.55	–62 18 02.5	20.73	2	–	–	249	17	–	–	249	13	282	5	284	9	–	–	–	PMNJ0719–6218
0738–6735	07 38 56.49	–67 35 50.6	19.65	2	–	–	255	18	346	17	396	8	434	7	531	16	2.2	0.2	14.3	PKS0738–674
0743–6726#	07 43 31.60	–67 26 25.8	16.71	2	–	–	1069	214	1360	68	1904	38	2109	42	5638	169	4.8	0.1	–	PKS0743–67
0744–6919	07 44 20.26	–69 19 07.3	21.65	2	237	53	323	23	363	18	330	6	322	6	414	12	2.4	0.2	<6.0	PKS0744–691
0746–6612	07 46 43.66	–66 12 51.4	19.32	2	–	–	[371]	27	168	8	–	–	–	–	2089	63	12.0	0.4	–	PKS0746–660
0806–6101	08 06 49.26	–61 01 29.8	>22	0	–	–	108	8	147	7	175	4	182	3	163	5	3.1	0.6	14.4	PMNJ0806–6101
0818–6634	08 18 49.39	–66 34 00.4	19.12	2	–	–	111	8	114	6	127	3	96	2	53	1	<2.7	–	<6.0	PMNJ0818–6634
0820–6814	08 20 11.23	–68 14 40.8	21.52	2	–	–	193	14	64	4	156	3	121	2	53	2	<4.2	–	49.9	PMNJ0820–6814
0835–5953	08 35 28.91	–59 53 11.6	>22	0	–	–	269	19	307	15	194	4	140	3	25	1	0.9	0.2	<6.0	PMNJ0835–5953
0842–6053	08 42 26.48	–60 53 50.4	19.98	1	–	–	318	22	320	16	376	7	398	4	745	22	1.2	0.2	<6.0	PMNJ0842–6053

Table 3 – continued

(1) Name	(2) Radio position (J2000)	(3) <i>B</i> (mag)	(4) <i>T</i>	(5) <i>S</i> <sub>18</sub> 2002	(6) <i>S</i> <sub>18</sub> 2003	(7) <i>S</i> <sub>18</sub> 2003	(8) <i>S</i> <sub>20</sub> 2004	(9) <i>S</i> <sub>8</sub> 2003	(10) <i>S</i> <sub>8</sub> 2003	(11) <i>S</i> <sub>8</sub> 2003	(12) <i>S</i> <sub>5</sub> 2003	(13) <i>S</i> <sub>5</sub> 2003	(14) <i>S</i> <sub>843</sub> SUMSS	(15) <i>S</i> <sub>843</sub> SUMSS	(16) <i>S</i> <sub>843</sub> SUMSS	(17) Polarization (per cent)	(18) Polarization ± (per cent)	(19) Variability (per cent)	(20) Alternate name	(21) Notes	
0845–6527	08 45 11.29	18.01	2	[237]	53	260	18	214	11	403	8	422	8	18	1	1.1	0.3	8.3	PMNJ0845–6527		
0846–6313	08 46 35.97	19.34	2	108	24	–	–	73	4	–	–	–	–	86	3	4.4	1.0	–	PMNJ0846–6313		
0847–6235	08 47 02.95	–62 13 34.8	19.16	2	–	117	8	108	5	140	3	149	3	191	6	2.7	0.8	<6.0	PMNJ0847–6235		
0901–6636	09 01 15.40	–66 36 33.8	21.38	1	[230]	51	160	11	165	8	249	5	266	5	193	6	4.5	0.6	<6.0	PKS0901–664	
0923–6648	09 23 47.51	–66 48 37.9	21.78	2	–	150	11	179	9	137	3	123	2	96	3	6.4	0.5	–	PKS0922–666		
0938–6556	09 38 41.82	–65 56 13.6	18.39	2	–	104	7	–	–	140	3	119	2	197	6	<1.7	–	–	PKS0937–657	QP	
0953–6924	09 53 20.48	–69 24 25.4	18.65	2	–	198	14	103	5	184	4	195	4	170	5	3.5	0.7	–	PKS0952–691		
1533–6837	15 33 34.61	–68 37 19.3	21.63	2	–	223	12	285	14	–	–	–	–	285	10	<1.3	–	11.1	PKS1528–684		
1542–6807	15 42 57.32	–68 07 49.8	16.77	2	–	125	16	58	3	–	–	–	–	243	8	<5.9	–	–	PMNJ1543–6808		
1546–6837	15 46 44.52	–68 37 29.3	19.51	2	[233]	52	131	9	503	25	–	–	–	206	8	2.8	0.2	58.4	PMNJ1546–6837		
1624–6809	16 24 18.55	–68 09 11.3	17.05	2	33.1	16	570	40	723	36	910	17	1473	27	1046	31	0.6	0.2	10.7	PKS1619–680	CQP* z = 1.360
1647–6438	16 47 37.91	–64 38 00.2	20.05	1	614	136	418	29	462	23	424	8	557	10	644	19	8.6	0.2	<6.0	MRC1642–645	CVE
1703–6212	17 03 36.78	–62 12 39.1	18.73	2	–	1572	110	1287	64	854	17	1223	22	731	22	0.5	0.1	8.6	MRC1659–621	CWE	
1703–6511	17 03 50.56	–65 11 06.2	18.10	2	[99]	22	–	135	7	–	–	–	–	345	10	2.2	0.6	–	PKS1658–651		
1709–6905	17 09 55.80	–69 05 22.6	20.34	1	–	122	9	148	7	70	2	86	2	56	2	<2.1	–	8.2	PMNJ1709–6905		
1721–6154	17 21 39.07	–61 54 42.8	18.91	2	[340]	75	381	27	297	15	288	6	285	5	310	9	2.5	0.3	11.3	PMNJ1721–6154	
1723–6500	17 23 41.12	–65 00 36.3	13.16	1	[2945]	654	2671	187	2817	141	2626	51	–	3724	112	<1.7	–	<6.0	NGC6328	CMWVP* z = 0.0142	
1726–6427	17 26 57.91	–64 27 52.4	>22	0	204	13	209	15	150	8	344	7	1041	19	4076	122	<1.8	–	15.6	MRC1722–644	CV
1735–6215	17 35 08.11	–62 15 21.2	19.59	2	[256]	57	403	28	300	15	262	5	403	7	696	21	1.1	0.3	13.7	MRC1730–622	
1736–5951	17 36 30.95	–59 51 58.3	21.51	2	236	62	181	13	192	10	151	3	242	4	269	8	2.5	0.4	<6.0	PKS1732–598	Q
1737–5921	17 37 19.80	–59 21 41.0	20.99	1	–	395	28	247	12	253	5	368	7	381	12	5.5	0.3	–	PMNJ1737–5921		
1743–6626	17 43 49.13	–66 26 27.5	20.76	2	176	39	124	9	192	10	74	2	117	2	209	6	2.7	0.5	20.9	PKS1738–664	
1749–6258	17 49 25.80	–62 58 17.8	19.08	1	182	40	181	13	186	9	111	2	162	3	244	7	2.4	0.4	<6.0	PMNJ1749–6258	
1754–6423	17 54 42.21	–64 23 45.3	19.15	2	83	18	–	–	103	5	–	–	–	177	5	<2.6	–	–	PMNJ1754–6423		
1759–5947	17 59 06.08	–59 47 01.1	>22	0	112	25	–	67	4	–	–	–	–	5626	169	13.0	0.9	–	PKS1754–59		
1803–6507	18 03 23.58	–65 07 36.8	18.19	1	[999]	222	1144	80	1314	66	771	19	–	637	19	0.8	0.1	<6.0	PKS1758–651	CWP	
1807–6413	18 07 54.03	–64 13 50.7	20.56	1	450	100	–	277	14	–	–	–	–	94	3	1.8	0.2	–	PMNJ1807–6413		
1807–7012#	18 07 14.76	–70 12 39.9	18.23	1	131	13	–	126	7	–	–	–	–	1199	36	13.2	1.7	–	PKS1801–702	M	
1819–6345	18 19 34.94	–63 45 48.5	16.80	1	1631	79	–	1825	91	–	–	–	–	20185	606	0.8	0.1	–	PKS1814–63		
1822–6359#	18 22 14.76	–63 59 24.4	>22	0	142	28	–	163	8	–	–	–	–	4935	181	6.1	0.7	–	PKS1817–64		
1824–6717#	18 24 34.21	–67 17 26.1	>22	0	228	46	–	310	20	–	–	–	–	3440	134	4.1	0.4	–	PKS1819–67		
1836–6649	18 36 59.40	–66 49 08.5	19.54	1	127	28	–	146	7	–	–	–	–	3260	98	4.7	0.4	–	PKS1831–668		
1840–6152	18 40 15.43	–61 52 06.3	21.96	2	245	54	282	20	254	13	–	–	–	191	6	1.1	0.2	<6.0	PKS1835–619		
1844–6808	18 44 11.82	–68 08 05.3	20.00	2	–	188	13	114	6	–	–	–	–	111	4	2.9	0.6	23.9	PMNJ1844–6808		
1852–6848	18 52 32.29	–68 48 16.1	>22	0	101	22	–	86	5	–	–	–	–	403	12	4.0	0.6	–	PKS1847–688		
1903–6749	19 03 01.32	–67 49 35.5	18.90	2	419	21	156	11	481	24	–	–	–	232	7	5.2	0.1	50.7	PMNJ1903–6749		
1906–6556	19 06 47.72	–65 56 41.1	>22	0	–	[264]	18	111	6	–	–	–	–	447	14	2.1	0.4	–	PKS1901–660		
1913–6950	19 13 31.25	–69 50 37.4	>22	0	282	63	317	22	192	10	–	–	–	100	3	<0.9	–	24.0	PMNJ1913–6928		
1916–6928	19 16 36.33	–69 28 33.7	>22	0	–	225	16	117	6	–	–	–	–	102	3	3.6	0.4	–	PMNJ1916–6928		
1917–6436	19 17 34.06	–64 35 43.8	20.55	2	–	116	8	64	4	–	–	–	–	102	3	6.5	0.7	–	PMNJ1917–6435		

Table 3 – continued

(1) Name	(2) Radio position (J2000)	(3) <i>B</i> (mag)	(4) <i>T</i>	(5) <i>S</i> <sub>18</sub> 2002	(6) <i>S</i> <sub>18</sub> 2003	(7) <i>S</i> <sub>18</sub> 2003	(8) <i>S</i> <sub>20</sub> 2004	(9) <i>S</i> <sub>20</sub> 2004	(10) <i>S</i> <sub>8</sub> 2003	(11) <i>S</i> <sub>8</sub> 2003	(12) <i>S</i> <sub>5</sub> 2003	(13) <i>S</i> <sub>5</sub> 2003	(14) <i>S</i> <sub>843</sub> SUMSS	(15) <i>S</i> <sub>843</sub> SUMSS	(16) ±	(17) Polarization ± (per cent)	(18) ±	(19) Variability (per cent)	(20) Alternate name	(21) Notes
1923–6320	19 23 24.64	21.42	2	–	–	184	13	127	6	–	–	–	–	412	13	1.8	0.4	17.6	PMNJ1923–6320	
1926–6242	19 26 58.09	18.64	2	133:	30	–	–	93	5	–	–	–	–	139	5	3.5	0.5	–		
1930–6056	19 30 06.07	20.57	2	675	150	819	57	572	29	–	–	–	–	696	21	3.1	0.1	17.0	PKS1925–610	CQP
1933–6942	19 33 31.22	19.94	2	388	86	–	–	259	13	–	–	–	–	744	22	1.2	0.2	–	PKS1928–698	QP
1939–6342	19 39 24.99	18.87	1	[1272]	350	1227	86	886	44	–	–	–	–	13722	412	<0.2	–	<6.0	PKS1934–63	CV* <i>z</i> = 0.183
1940–6907	19 40 26.09	>22	0	[568]	126	556	39	442	22	–	–	–	–	1705	51	2.1	0.1	10.3	PKS1935–692	CQV <i>z</i> = 3.154
1940–6527	19 40 38.91	20.75	2	–	–	242	13	282	14	–	–	–	–	244	7	0.7	0.2	<6.0	PMNJ1940–6527	
1941–6211	19 41 21.74	21.12	1	502:	111	390	27	348	17	–	–	–	–	1832	55	4.0	0.2	<6.0	PKS1936–623	QP*
1942–7015	19 42 45.52	19.29	2	111	25	–	–	75	4	–	–	–	–	80	3	2.6	0.7	–	PMNJ1942–7015	
2004–6347	20 04 29.52	19.35	2	456	13	355	25	369	18	369	8	560	10	749	23	1.5	0.2	<6.0	PMNJ2004–6347	C
2015–6712	20 15 00.00	19.02	1	[73]	16	–	–	214	11	–	–	–	–	39	2	<1.0	–	–	PMNJ2014–6713	M
2017–6824	20 17 29.30	19.29	1	–	–	175	12	164	8	175	9	227	4	243	7	4.3	0.4	<6.0	PKS2012–685	QP
2021–6124	20 21 01.34	20.45	1	183	41	163	11	200	10	321	7	468	9	1071	32	4.2	0.3	14.0	PKS2016–615	CQ
2024–6458	20 24 46.30	20.79	2	–	–	[267]	21	192	10	–	–	–	–	126	4	2.7	0.3	–	PMNJ2024–6458	
2027–7007	20 27 24.54	19.19	2	[308]	68	–	–	233	12	–	–	–	–	1041	31	1.7	0.3	–	PKS2022–702	Q <i>z</i> = 0.697
2035–6846	20 35 48.85	19.27	2	–	–	570	40	457	23	651	13	745	14	299	9	4.2	0.2	9.8	PKS2030–689	QWP
2035–6602	20 35 51.46	19.24	2	–	–	320	22	259	13	325	7	386	7	355	11	3.6	0.2	9.2	PMNJ2035–6602	
2046–6527	20 46 49.64	21.58	2	116	26	–	–	130	7	–	–	–	–	36	1	<1.5	–	–	PMNJ2046–6527	
2048–6804	20 48 23.81	18.20	2	–	–	114	8	104	5	122	3	170	3	349	11	1.9	0.5	<6.0	PKS2043–682	C
2052–6523	20 52 06.64	17.29	2	–	–	275	19	228	11	275	15	375	7	551	17	1.3	0.3	7.9	PKS2047–655	QP <i>z</i> = 2.320
2053–6255	20 53 05.62	21.19	2	–	–	236	17	280	14	269	5	313	6	171	5	1.8	0.2	6.9	PMNJ2053–6255	
2059–6745	20 59 09.59	17.70	1	90	20	–	–	104	5	–	–	–	–	2456	9	<2.0	–	–	PMNJ2059–6745	M
2106–6547	21 06 59.73	20.88	2	303	67	315	22	305	15	424	8	585	11	1555	47	<0.7	–	<6.0	PKS2102–659	C
2114–6851	21 14 13.46	19.58	2	140:	31	189	13	223	11	225	5	285	5	510	15	2.6	0.3	6.5	PKS2109–690	Q <i>z</i> = 2.910
2121–6111	21 21 04.10	18.75	2	214:	48	287	20	357	18	367	7	476	9	966	29	2.1	0.2	9.6	MRC2117–614	C
2121–6404	21 21 55.05	21.19	2	–	–	263:	18	164	8	354	7	588	11	2081	62	<1.1	–	–	PKS2117–64	C
2124–6028	21 24 02.94	17.32	2	–	–	[323]	23	134	7	–	–	–	–	35	1	<1.5	–	–		
2134–6513	21 34 13.25	19.21	2	–	–	166	12	179	9	136	3	142	3	213	7	6.2	0.4	<6.0	PKS2130–654	
2136–6335	21 36 22.09	19.77	2	–	–	238	17	385	19	180	4	144	3	160	5	0.7	0.2	23.0	PMNJ2136–6335	
2141–6411	21 41 46.50	19.58	2	–	–	200	14	217	11	153	3	152	3	176	5	5.8	0.3	<6.0	PMNJ2141–6411	
2150–6802	21 50 13.43	20.83	2	215:	48	179	13	246	12	230	5	229	4	126	4	1.0	0.2	14.9	PMNJ2150–6803	
2156–6331	21 56 49.11	19.98	2	97	22	–	–	141	7	–	–	–	–	57	2	<1.6	–	–	PMNJ2156–6331	
2157–6941#	21 57 05.45	13.85	1	1821	304	[759]	53	1490	75	2760	59	8300	171	41200	1455	2.4	0.1	–	ESO075–G41	IXWM <i>z</i> = 0.0283
2203–6130	22 03 59.63	19.86	1	249	55	282:	20	289	14	264	5	346	6	441	13	3.5	0.2	–	PKS2200–617	QP
2208–6325	22 08 47.15	18.41	2	[298]	66	335	23	337	17	453	9	634	12	1429	43	4.2	0.2	<6.0	PKS2204–63	CQ <i>z</i> = 0.618
2213–6330	22 13 34.73	18.52	2	325	72	322	23	334	17	223	5	209	4	631	25	1.4	0.2	<6.0	PKS2210–637	X
2215–6609	22 15 45.26	21.19	2	110	24	–	–	134	7	–	–	–	–	761	23	4.4	0.5	–	PKS2212–664	
2229–6910	22 29 00.21	19.85	2	–	–	596	42	626	31	549	11	491	9	400	12	0.8	0.1	<6.0	PKS2225–694	QP
2230–6310	22 30 10.29	19.85	2	187	42	144	10	156	8	184	4	193	4	231	7	3.4	0.4	<6.0	PMNJ2230–6310	
2231–6231	22 31 07.91	20.25	1	[395]	88	316	22	249	12	346	7	332	6	267	8	1.5	0.2	10.7	PKS2227–627	

Table 3 – continued

(1) Name	(2) Radio position (J2000)	(3) $B$ (mag)	(4) $T$	(5) $S_{18}$ 2002	(6) $S_{18}$ 2003	(7) $S_{18}$ 2003	(8) $S_{20}$ 2004	(9) $S_{20}$ 2004	(10) $S_8$ 2003	(11) $S_8$ 2003	(12) $S_5$ 2003	(13) $S_5$ 2003	(14) $S_{43}$ SUMSS	(15) $S_{43}$ SUMSS	(16) $\pm$	(17) Polarization (per cent)	(18) $\pm$	(19) Variability (per cent)	(20) Alternate name	(21) Notes
2243–6250	22 43 07.78	18.19	2	–	–	199	14	224	11	224	5	194	4	111	3	1.2	0.2	<6.0	PKS2239–631	P
2254–5926	22 54 56.77	19.80	2	–	–	239	17	194	10	159	3	157	3	159	5	1.8	0.3	–	PKS2251–596	P
2256–6533	22 56 24.89	16.90	2	–	–	114	8	99	5	125	3	150	3	349	10	3.0	0.6	<6.0	PMN12256–6533	
2301–5913	23 01 36.19	17.72	1	–	–	–	–	117	6	–	–	–	–	61	2	<2.3	–	–	PMN12301–5913	XM $z = 0.149$
2303–6807	23 03 43.54	16.26	2	924	205	1067	75	939	47	1013	22	1035	22	759	29	3.2	0.1	10.3	PKS2300–683	QX $z = 0.512$
2306–6521	23 06 59.43	>22	0	104	23	–	–	96	5	–	–	–	–	372	11	<2.5	–	–	PKS2303–656	P $z = 0.470$
2310–5941	23 10 28.48	18.35	1	109	24	[204]	16	134	7	180	4	162	3	74	4	<2.2	–	–	IRAS23074–5957	MI $z = 0.1415$
2312–6607	23 12 58.80	18.77	2	111	25	287	20	156	8	132	3	142	3	107	3	1.6	0.5	–	PMN12312–6607	
2327–6644	23 27 45.38	>22	0	184	25	187	13	176	9	240	5	272	5	470	14	4.7	0.4	<6.0	PKS2324–670	P
2335–6637	23 35 12.26	>22	0	118	26	–	–	119	6	–	–	–	–	3422	127	9.9	0.8	–	PKS2332–66	
2348–6049	23 48 26.00	21.17	2	–	–	182	13	137	7	178	4	180	3	217	7	3.5	0.7	13.1	PKS2345–611	
2356–6820	23 56 00.75	17.61	2	671	97	795	56	781	39	588	11	702	13	1126	34	<0.4	–	<6.0	PKS2353–68	CQP* $z = 1.716$
2358–6052#	23 58 45.15	16.61	1	680	108	240	17	248	12	344	7	820	15	2900	2900	5.2	–	–	PKS2356–61(N)	MWV $z = 0.0963$
2359–6057#	23 59 22.77	16.61	1	275	61	–	–	–	–	–	–	–	–	–	–	–	–	–	PKS2356–61(S)	

### 3.4 Extended sources at 20 GHz

The great majority of the sources detected in the 20 GHz pilot survey are unresolved in our follow-up images at 5, 8 and 20 GHz. The source-detection algorithm used in the pilot survey was optimized for point sources, and there will be some bias against extended sources with angular sizes larger than about 30 arcsec. For sources larger than 1 arcmin in size, the total flux densities listed in Table 3 may also be underestimated.

Only 11 of the 173 sources in Table 3 were resolved in our (15-arcsec resolution) 20 GHz images. The overall properties of extended sources in the current sample are as follows.

(i) Four objects, J0103–6439, J2157–6941 and J2358–6052/J2359–6057, are very extended double-lobed radio sources which are too large to be imaged with these ATCA snapshots. As a result, the total flux densities listed in Table 3 are lower limits to the correct value.

(ii) Another seven sources are resolved in our ATCA images, but still lie within the 2.2 arcmin primary beam of the ATCA at 20 GHz. Details of these objects are given in Appendix A.

(iii) Five of the extended sources (J0103–6439, J0121–6309, J0257–6112, J0743–6726 and J2157–6941) have a flat-spectrum core which dominates the flux density at 20 GHz.

Since the number of extended sources is small, and they appear to be somewhat diverse in nature, we defer any detailed discussion of the extended radio-source population to a later paper.

### 3.5 Optical identification of the 20 GHz sources

We examined all the sources in Table 3 in the SuperCOSMOS online catalogue and images (Hambly et al. 2001). An optical object was accepted as the correct ID for a 20 GHz radio source if it was brighter than  $b_j = 22$  mag and lay within 2.5 arcsec of the radio position. For one source in Table 3 (J0715–6829) the optical image was saturated by light from a nearby 11th magnitude star and so no identification could be attempted. Of the remaining 172 sources, 146 (85 per cent) had an optical ID which met the criteria listed above. Monte Carlo tests (based on matching the SuperCOSMOS catalogue with radio positions randomly offset from those in Table 3) imply that at least 97 per cent of these IDs are likely to be genuine associations, rather than a chance alignment with a foreground or background object.

As can be seen from Fig. 4, the majority (65 per cent) of radio sources selected at 20 GHz have stellar IDs on the DSS  $B$  images, and are candidate QSOs or BL Lac objects. 20 per cent of the radio sample are identified with galaxies and 15 per cent are faint objects or blank fields. The overall optical identification rate of 85 per cent for radio sources selected at 20 GHz is significantly higher than the identification rate for bright radio sources selected at 1.4 GHz (typically  $\sim 30$  per cent above  $B \sim 22$  mag), but is closer to that found by Bolton et al. (2004) for a flux-limited sample of radio sources selected at 15 GHz, as discussed in Section 8.1.1.

Fig. 5 shows the relation between  $b_j$  magnitude and redshift for the 22 sources (13 per cent of the objects in Fig. 4) which currently have a published redshift. A representative sample of nearby radio galaxies (Sadler et al. 2002) selected from the 2dF Galaxy Redshift Survey (2dFGRS; Colless et al. 2001) is shown for comparison. Galaxies detected in our 20-GHz survey appear to span a narrow range in optical luminosity similar to that seen in nearby radio galaxies selected at lower frequencies, though we caution that the sub-sample of sources with published redshifts is inhomogeneous

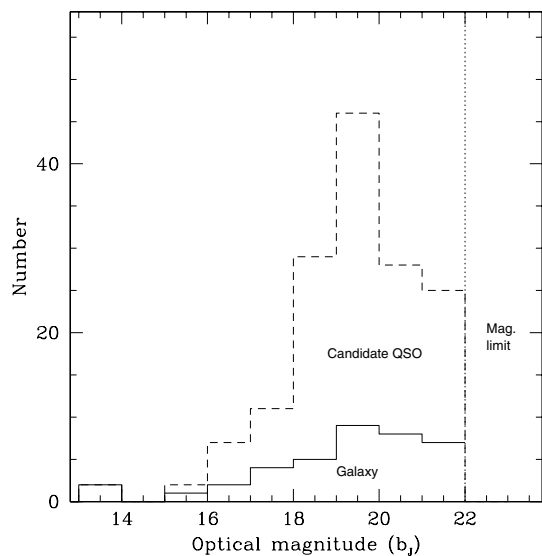


**Figure 4.** Optical identifications for the 20 GHz radio sources in Table 3. Galaxies and stellar objects (QSO candidates) are shown separately. Only 27 sources (13 per cent of the sample) are unidentified down to  $b_j < 22$  mag.

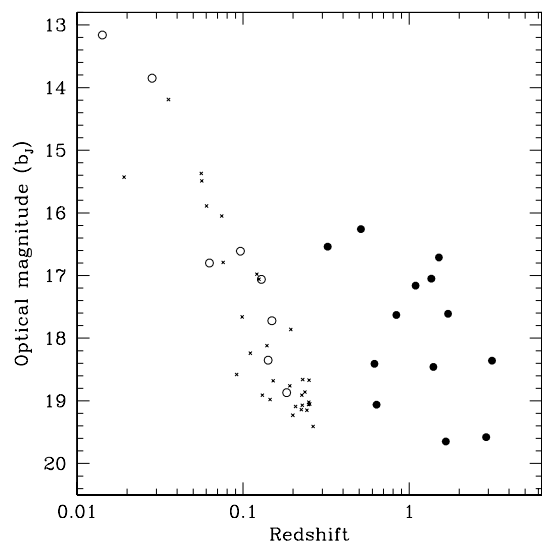


**Figure 5.** Relation between SuperCOSMOS  $b_j$  magnitude and redshift for those objects in our sample which have a published redshift. Open circles show galaxies from the 20 GHz sample and filled circles QSOs. The small crosses show a representative subsample of 2dFGRS radio galaxies selected at 1.4 GHz (Sadler et al. 2002). The highest redshift so far measured for an object in this sample is for J1940–6907, a QSO at  $z = 3.154$ .

in nature and may be biased in luminosity and/or redshift distribution because redshifts are easier to measure for brighter galaxies and QSOs.

#### 4 RELIABILITY AND REPRODUCIBILITY OF THE SCANNING SURVEY

As noted earlier, the fact that our pilot survey scanned the same area of sky in both 2002 and 2003 provides an important test of the observational techniques to be used for the full AT20G survey (i.e. fast scans of large areas of sky, followed by imaging of candidate

**Table 4.** The fraction of sources detected at 18 GHz in the 2002 scans which were independently detected in the 2003 scans of the pilot survey area.

$S_{18}$ (mJy)	Observed in 2002	Recovered in 2003	Fraction recovered (per cent)
<100	6	0	0
101–125	13	4	31
126–150	8	5	63
151–200	12	12	100
>200	50	47	94

sources identified in the scans). In particular, how good a job does the scanning technique do in finding genuine sources down to the nominal detection limit, and how reproducible are the source lists produced by this technique?

Table 4 shows the recovery rate in 2003 of sources detected in the 2002 pilot survey scans. As might be expected (since the nominal detection limit of the 2003 survey was 100 mJy), none of the weakest ( $S_{18} < 100$  mJy) sources detected in 2002 was recovered in the 2003 scans, but the recovery rate rises to 95 per cent for sources with measured flux densities above 150 mJy in 2002. We checked the three sources above 150 mJy which were not recovered in 2003. In all cases these sources were visible in the raw data scans, so had not decreased in flux density to below the survey limit. Instead, they were missed from the follow-up imaging program because of deficiencies in the source-detection algorithm for extended sources or sources with nearby bad data points. For the full AT20G survey, we will use an improved source-detection algorithm.

Fig. 1 compares the 18 GHz flux densities measured in 2002 and 2003 for sources detected in both years. It implies that the flux-density scales are in good agreement, and gives some first hints that the general variability level at 18 GHz is modest (though the large error bars on the 2002 flux densities mean that this is not a very useful data set for studying variability in a quantitative way). We therefore conclude that the scanning technique produces a reliable and robust catalogue of sources, in the sense that rescanning an area of sky will produce essentially the same source catalogue each time.

## 5 RADIO SPECTRA OF THE 20 GHz SOURCES

### 5.1 Representative radio spectra at 0.8–20 GHz

Fig. 6 shows some representative radio spectra for sources in our sample. It is clear we see a wide variety of spectral shapes, most of which cannot be fitted by a single power law over the frequency range 1–20 GHz. We can distinguish four main kinds of spectra.

- (i) Sources with steep (falling) spectra over the whole range 843 MHz to 20 GHz (e.g. J0408–6545 in Fig. 6).
- (ii) Sources with peaked (GPS) spectra, in which the flux density rises at low frequency and falls at high frequency (e.g. J0201–6638).
- (iii) Sources with inverted (rising) radio spectra over the whole frequency range (e.g. J0113–6753).
- (iv) Sources with an upturn in their spectrum, where the flux density is falling at lower frequencies, but then turns up and begins to rise above 5–8 GHz (e.g. J2213–6330).

In addition, a small number of sources have flat radio spectra in which the flux density is essentially constant over the entire frequency range observed (e.g. J0220–6330 in Fig. 6).

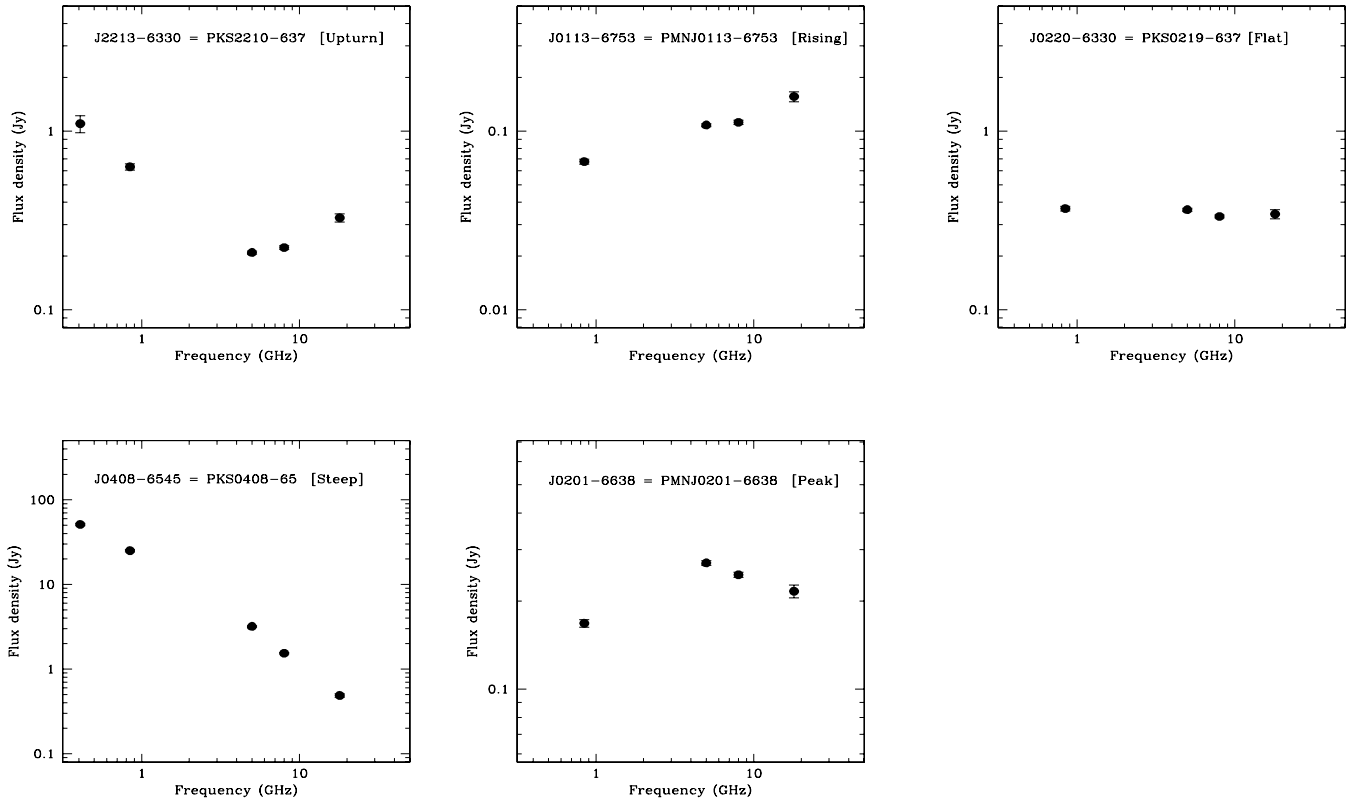


**Figure 6.** Examples of radio spectra for each of the four spectral classes identified in the text (Upturn, Rising, Steep and Peak), together with a spectrum classified as Flat ( $|\alpha| < 0.1$  for both 0.84–5 GHz and 8–20 GHz). Where available, a 408 MHz flux density from the MRC (Large et al. 1981) is plotted in addition to the data from Table 3.

The radio spectral index

$$\alpha = \frac{\log S_1 - \log S_2}{\log \nu_1 - \log \nu_2},$$

where  $S_1$  and  $S_2$  are the measured flux densities at frequencies  $\nu_1$  and  $\nu_2$ , is commonly used to characterize radio-source populations at centimetre wavelengths (frequencies of 1–5 GHz) where many large-area radio surveys have been carried out.

At centimetre wavelengths the radio emission from flat-spectrum ( $\alpha > -0.5$ ) objects is dominated by a compact, self-absorbed component, while steep-spectrum objects ( $\alpha < -0.5$ ) are dominated by optically thin synchrotron emission. The flat- and steep-spectrum populations are usually considered separately when modelling the cosmic evolution of radio sources (e.g. Peacock & Gull 1981; Peacock 1985).

As pointed out by Peacock (1985), the radio spectral index is only valid as a diagnostic tool if it is measured over a frequency interval small enough that the effects of spectral curvature can be neglected. Because many of the sources in our sample have significant spectra curvature over the frequency range 1–20 GHz, we therefore use a ‘radio two-colour’ diagram, rather than a single spectral index, to characterize the high-frequency radio-source population. As discussed in the next section, this diagram compares a low-frequency spectral index  $\alpha_L$  (which corresponds closely to the spectral index traditionally used to separate flat- and steep-spectrum radio sources) with a high-frequency spectral index  $\alpha_H$  which measures the spectral shape above 8 GHz.

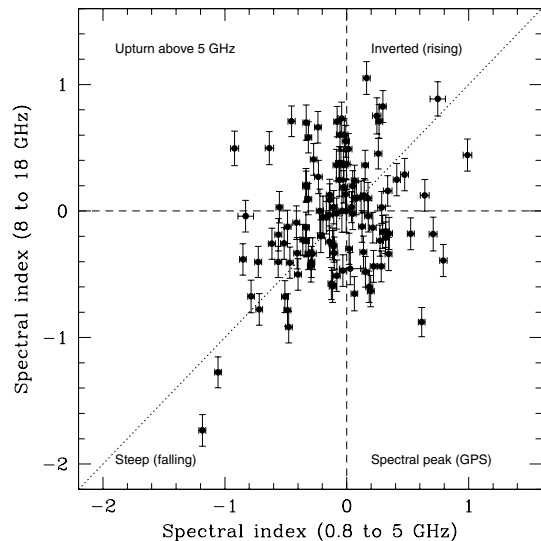


**Figure 7.** Radio ‘two-colour diagram’ for the 119 extragalactic sources in Table 3 which have good-quality multifrequency observations made in late 2003.

## 5.2 The radio two-colour diagram

Fig. 7 shows the radio two-colour diagram, which compares the spectral indices  $\alpha_L$  (at 0.84–5 GHz) and  $\alpha_H$  (at 8–18 GHz) for sources selected at 20 GHz. Such a diagram is analogous to the two-colour diagram used in optical astronomy to characterize the

broad-band continuum properties of stars and galaxies. The diagram shown in Fig. 7 has the advantage that the axes (and error bars) are independent, and the four main spectral classes identified in Fig. 6 correspond to the four quadrants in the two-colour diagram. The dotted line shows the relation for galaxies whose spectra follow a single power law from 0.8 to 18 GHz. Only a small fraction of sources fall on or near the dotted line, and it is clear that  $\alpha_L$  and  $\alpha_H$  are not strongly correlated.

As can be seen from Table 5, over 30 per cent of the sources in Fig. 7 have flat or inverted spectra between 8 and 20 GHz (i.e.  $\alpha_H > 0$ ), and more than half of these (like J2213–6330 in Fig. 6) have steep radio spectra below 5 GHz and would not have been predicted as strong 20 GHz sources on the basis of their low-frequency spectra. In contrast, many sources with flat or inverted spectra below 5 GHz turn over and become steep above 8 GHz.

## 6 VARIABILITY AT 20 GHz

### 6.1 Previous work

As mentioned in the introduction, there have been only a few studies of radio-source variability at frequencies above 5 GHz. Owen, Spangler & Cotton (1980) investigated the variability of a sample of strong ( $S_{90} > 1$  Jy) flat-spectrum sources at 5 and 90 GHz over a one-year period. They found that these sources were only slightly more variable at 90 GHz than at 5 GHz, in contrast to what they had expected. Tingay et al. (2003) also found that the level of variability of strong, compact radio sources increased only moderately with frequency. They used the ATCA to monitor a sample of 202 sources from the VSOP all-sky survey at 1.4, 2.5, 4.8 and 8.6 GHz, and found a median variability of 6 per cent at 1.4 GHz and 9 per cent at 8.6 GHz over a time-scale of 3–4 yr. Barvainis et al. (2005) found similar variability levels at 8.5 GHz for a sample of radio-loud and radio-quiet QSOs observed at the Very Large Array.

These studies are based largely on objects pre-selected at lower frequencies, and may not give a complete picture of the variability of the 20 GHz source population as a whole.

### 6.2 Quantifying variability

Following Barvainis et al. (2005) and Akritas & Bershad (1996), we use a debiased variability index which takes into account the uncertainties in individual flux-density measurements. We define the fractional variability index,  $V_{\text{rms}}$  by

$$V_{\text{rms}} = \frac{100}{\langle S \rangle} \sqrt{\frac{\sum [S_i - \langle S \rangle]^2 - \sum \sigma_i^2}{N}},$$

where  $S_i$  are individual flux-density measurements for the same source,  $\sigma_i$  is the error on each measurement,  $N$  is the number of data points, and  $\langle S \rangle$  is the mean flux density. We follow Barvainis

**Table 5.** Distribution of our sample in the five spectral classes defined in Section 4.1 and Fig. 6.

Spectrum	How defined	Number	Fraction (per cent)
Steep	$\alpha_L < 0, \alpha_H < 0$	32	$32 \pm 6$
Upturn	$\alpha_L < 0, \alpha_H > 0$	22	$22 \pm 5$
Rising (inverted)	$\alpha_L > 0, \alpha_H > 0$	18	$18 \pm 4$
Peak	$\alpha_L > 0, \alpha_H < 0$	23	$23 \pm 4$
Flat	$-0.1 < (\alpha_L, \alpha_H) < 0.1$	6	$6 \pm 2$
Total		101	

et al. (2005) in setting the variability index to be negative when the value inside the square root becomes negative. However, rather than listing negative values of the variability index, as was done by Barvainis et al. (2005), we used the distribution of positive and negative values to define the minimum level of variability which is detectable in our data. This was found to be 6 per cent, so for all sources with a variability index below this we list the debiased variability index as  $< 6.0$  per cent.

We used only the 2003 and 2004 data sets in our variability analysis, since these have significantly smaller flux-density errors than the 2002 data. The 2003 imaging observations were made at 18 GHz and the 2004 observations at 20 GHz, so there is a possibility of measuring spurious ‘variability’ for sources which have steeply falling radio spectra at 18–20 GHz. To overcome this, we used the 8–18 GHz spectral index from Table 3 to extrapolate the 2003 measurements to 20 GHz for the small number of sources in Table 3 which have  $\alpha < -0.7$  between 8 and 18 GHz. As discussed in Section 2.3, different ATCA primary flux calibrators were also used for the 2003 and 2004 observing runs. Since there appears to be no systematic offset between our 2003 and 2004 flux density measurements at 20 GHz (see Fig. 2), we do not believe that this has introduced any spurious ‘variability’ into our data set.

Fig. 8 plots the debiased variability index against flux density. Although several of the strongest sources in our sample are also highly variable (in particular 0623–6436, 1546–6837 and 1903–6749 in Table 3), there appears to be no strong correlation between

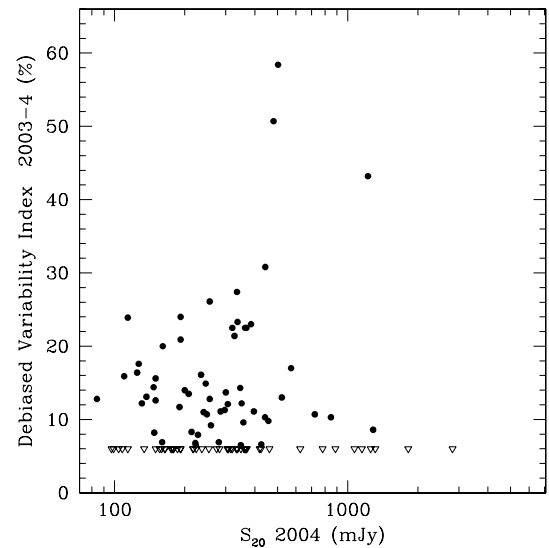


**Figure 8.** Debiased variability index at 20 GHz, measured from 2003 to 2004 for 121 sources observed at both epochs. Variability of 6 per cent or more over this one-year interval is detectable in the current data set.

**Table 6.** Distribution of the debiased variability index at 20 GHz for radio sources in our sample.

Debiased variability (per cent)	$n$	Fraction (per cent)
$< 10$	63	$58 \pm 7$
10–20	29	$27 \pm 5$
20–30	11	$10 \pm 3$
$> 30$	5	$5 \pm 2$
Total	108	

**Table 7.** *WMAP* sources at Dec.  $-60^\circ$  to  $-70^\circ$ , and with Galactic latitude  $|b| > 10^\circ$ . The five *WMAP* frequency bands are *K* (23 GHz), *K<sub>a</sub>* (33 GHz), *Q* (41 GHz), *V* (61 GHz) and *W* (94 GHz), and the flux densities are from Bennett et al. (2003). Only one of our sources (J2035–6846) was detected by *WMAP* at 94 GHz, so *W*-band data are not included in this table.  $\alpha_H$  is the 8–20 GHz spectral index measured in this paper (see Section 4), and  $\alpha_{\text{WMAP}}$  is the *WMAP* spectral index quoted by Bennett et al. (2003).

Name	<i>WMAP</i> catalogue no.	$S_{20}$ ATCA (Jy)	$S_{23}$	$S_{33}$ <i>WMAP</i> (Jy)	$S_{41}$	$S_{61}$	$\alpha_H$	$\alpha_{\text{WMAP}}$	Polarization (per cent)	Variability (per cent)
0303–6211	162	$1.26 \pm 0.09$	$1.5 \pm 0.1$	$1.6 \pm 0.2$	$1.5 \pm 0.2$	$1.7 \pm 0.3$	$-0.51 \pm 0.12$	$+0.1 \pm 0.4$	2.5	<6.0
0309–6058	160	$1.15 \pm 0.08$	$1.3 \pm 0.1$	–	–	$1.6 \pm 0.5$	$-0.04 \pm 0.12$	$+0.2 \pm 0.8$	0.8	<6.0
0506–6109	154	$1.82 \pm 0.12$	$2.9 \pm 0.09$	$2.4 \pm 0.1$	$2.0 \pm 0.2$	$1.5 \pm 0.3$	$+0.09 \pm 0.12$	$-0.4 \pm 0.3$	1.2	<6.0
0546–6415	156	$0.36 \pm 0.03$	$0.8 \pm 0.06$	$0.6 \pm 0.09$	$0.6 \pm 0.1$	–	$+0.25 \pm 0.13$	$-0.6 \pm 0.8$	<0.6	22.5
0743–6726	161	$1.07 \pm 0.08$	$1.6 \pm 0.1$	$1.0 \pm 0.1$	$1.0 \pm 0.2$	–	$-0.38 \pm 0.12$	$-1.1 \pm 0.6$	4.8	<6.0
1703–6212	198	$1.29 \pm 0.09$	$1.9 \pm 0.1$	$2.0 \pm 0.2$	$2.3 \pm 0.2$	$2.0 \pm 0.3$	$+0.83 \pm 0.13$	$+0.1 \pm 0.3$	0.5	<6.0
1723–6500	196	$2.82 \pm 0.20$	$2.1 \pm 0.1$	$2.0 \pm 0.2$	$1.6 \pm 0.2$	–	$+0.02 \pm 0.12$	$-0.3 \pm 0.4$	<1.7	<6.0
1803–6507	199	$1.31 \pm 0.09$	$1.2 \pm 0.1$	$1.4 \pm 0.2$	$1.5 \pm 0.2$	$1.2 \pm 0.3$	$+0.53 \pm 0.12$	$+0.2 \pm 0.5$	0.8	<6.0
1819–6345	200	$1.83 \pm 0.13$	$1.7 \pm 0.1$	$1.2 \pm 0.2$	$1.1 \pm 0.2$	$1.4 \pm 0.5$	–	$-0.7 \pm 0.5$	0.8	–
2035–6846	194	$0.46 \pm 0.03$	$1.0 \pm 0.2$	$1.3 \pm 0.2$	$0.9 \pm 0.2$	–	$-0.18 \pm 0.13$	$+0.4 \pm 0.6$	4.2	9.8
2157–6941	190	$1.99 \pm 0.11$	$3.6 \pm 0.1$	$2.9 \pm 0.2$	$2.6 \pm 0.2$	$2.2 \pm 0.4$	–	$-0.6 \pm 0.2$	2.4	–
2359–6052	187	>0.9	$1.8 \pm 0.1$	–	$1.3 \pm 0.1$	–	–	$-0.5 \pm 0.5$	5.2	–

variability and flux density for the sample as a whole. For example, the generalized Kendall’s tau correlation implemented in the ASURV statistical package for censored data (Isobe, Feigelson & Nelson 1986) has a value of 1.66, corresponding to a probability of 9.7 per cent that no correlation is present. Table 6 shows the distribution of the debiased variability index measured for sources in Table 3 over a one-year time-span from 2003 October to 2004 October. The majority of sources (58 per cent) vary by less than 10 per cent in 20 GHz flux density over this period, and only five sources varied by more than 30 per cent. The median debiased variability index at 20 GHz is 6.9 per cent.

## 7 SOURCES DETECTED BY WMAP

Table 7 lists the sources in our sample which were also detected by the *WMAP* satellite (Bennett et al. 2003) at up to five frequencies between 23 and 94 GHz. All 12 *WMAP* sources with Galactic latitude  $|b| > 10^\circ$  in the Dec. zone  $-60^\circ$  to  $-70^\circ$  were detected in our 20-GHz survey, and Fig. 9 shows that there is generally good agreement between the 23 GHz flux densities measured by *WMAP* and the 20 GHz values measured in this study. Of the 10 sources in our survey with  $S_{20} > 1$  Jy, nine are also detected by *WMAP* at 23 GHz. The sole exception is 0623–6436, a Seyfert 1 galaxy which appears to be strongly variable at 20 GHz (it has a variability index of 43 per cent in Table 3).

## 8 DISCUSSION AND CONCLUSIONS

Our aim in this paper has been to present some first results on the polarization and variability of radio sources selected at 20 GHz, and to outline some methodology which will also be useful in analysing data from the much larger ATCA 20 GHz (AT20G) survey which is now in progress. We now summarize and discuss the main results from our pilot survey of 173 sources selected to have flux densities above 100 mJy at 20 GHz.

### 8.1 Radio-source populations at 20 GHz

#### 8.1.1 Comparison with surveys at 15 GHz

Our survey is complementary to the recent 15 GHz studies of Taylor et al. (2001) and Bolton et al. (2004), since we cover a significantly larger area of sky, but at a somewhat higher flux-density level. It is

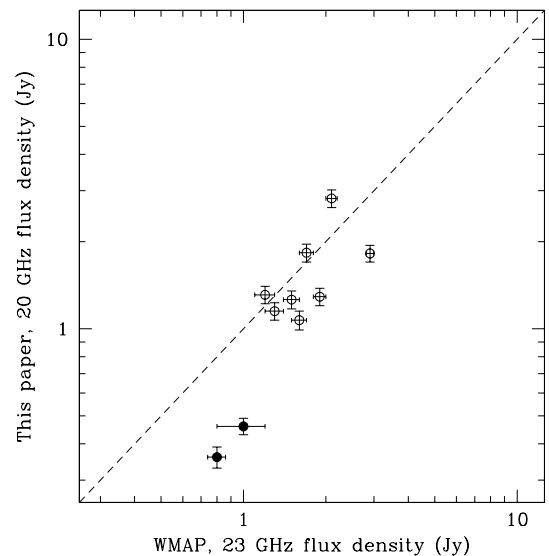


**Figure 9.** Comparison of our 20 GHz flux densities with the 23 GHz flux densities measured by *WMAP* for sources in common. The two filled circles show the objects for which we measured flux-density variability over the period 2003–04, as discussed in Section 5.

therefore interesting to compare some of our results with those in the 15-GHz surveys.

In Section 5, we used a radio two-colour diagram to characterize the spectra of sources selected at 20 GHz, and showed that most of these sources have significant spectral curvature over the range 0.8–20 GHz. Similar results were found by Bolton et al. (2004), who studied the 1.4–43 GHz radio spectra of 176 sources detected at 15 GHz in a blind survey of about 200 deg<sup>2</sup> of sky. Bolton et al. (2004) found that 20–30 per cent of their sources had rising spectra at 1–5 GHz, with the fraction increasing to 39 per cent for sources with  $S_{15} > 150$  mJy. Many of these sources had a spectral peak (turnover) above 5 GHz. For our sample selected at 20 GHz, 39 per cent of sources with  $S_{20} > 100$  mJy have rising spectra between 0.8 and 5.0 GHz (i.e.  $\alpha_L > 0.1$  in Table 5), with the majority of these showing a spectral peak above 5 GHz. Radio sources selected at 20 GHz therefore appear to have similar spectral

**Table 8.** Comparison of the optical properties of radio sources selected in high-frequency flux-limited surveys. The 15 GHz values are from Bolton et al. (2004) and the 20 GHz data from this paper.

Frequency (GHz)	Flux density limit	Median <i>b</i> mag	Fraction with an optical ID at <i>b</i> < 21 mag (per cent)
15	>25 mJy	21.6	52 ± 7 (64/124)
15	>60 mJy	20.9	61 ± 9 (43/70)
20	>100 mJy	19.8	82 ± 8 (118/144)
20	>500 mJy	18.9	93 ± 19 (25/27)

properties to sources selected at the slightly lower frequency of 15 GHz.

As noted in Section 3.5, the optical identification rate for sources selected at 20 GHz is significantly higher than has been found in surveys to similar flux limits at 1.4 GHz. In contrast to low frequencies, where the strongest radio sources are mostly distant, powerful radio galaxies (e.g. Jackson & Wall 1999), the strongest sources at 20 GHz appear to be mainly QSOs. A direct comparison with the optical results of Bolton et al. (2004) is not completely straightforward, since they made most of their optical identifications in the *R* band rather than *B* band, and did not explicitly distinguish between galaxies and candidate QSOs. However, we can directly compare our overall identification rate on the blue SuperCOSMOS DSS images with that found by Bolton et al. (2004) in the blue Palomar *O*-band DSS images, as shown in Table 8. Our results confirm the trend found by Bolton et al. (2004) for brighter 15–20 GHz sources to have a higher optical ID rate and brighter optical counterparts.

### 8.1.2 Comparison with predictions from low-frequency studies

Taylor et al. (2001) have noted that, as a result of spectral curvature, the radio-source population at 15 GHz cannot be reliably predicted by extrapolation from surveys at frequencies of 1–5 GHz. Of the sources they expected to detect at 15 GHz, based on extrapolation of the spectral index measured from the NVSS catalogue at 1.4 GHz and GB6 catalogue at 5 GHz, only 45 per cent (55/122) were actually seen. Furthermore, roughly 10 per cent of the sources they detected at 15 GHz were not predicted by this method.

We attempted to predict the observed source population in our survey region above 100 mJy at 20 GHz by extrapolating the radio spectral indices measured from the 0.84 GHz SUMSS and 4.85 GHz PMN surveys. For a subset of our survey area covering about 250 deg<sup>2</sup> well away from the Galactic plane, we detected 33 per cent (28/84) of the sources predicted from extrapolation of the 0.8–5 GHz spectral indices. Conversely, 18 per cent (6/34) of the sources we actually detected at 20 GHz were not predicted by the low-frequency extrapolation. We therefore confirm the findings of Taylor et al. (2001) that neither the existence nor the flux density of a 15–20 GHz source can be reliably predicted by extrapolating the results of surveys at lower frequencies, and show that this is also the case at higher flux densities than were probed by the Taylor et al. (2001) survey.

### 8.1.3 Phase calibrators for ALMA?

The results of the previous section are relevant to the planned calibration strategy for the ALMA millimetre array now under construction in Chile. ALMA will operate at 90–720 GHz, and the aim is to calibrate the data by fast-switching between a program source

and a calibrator less than 1°–2° away. The surface density of currently known calibrators at 90 GHz is far lower than this, so large numbers of new calibrators will need to be found. The currently planned strategy for this (Holdaway, Carilli & Laing 2004) is to select candidates by extrapolation from existing 1–5 GHz source catalogues. Our results, and those of Taylor et al. (2001) imply that such a strategy has at best a 30 per cent success rate in selecting sources at 20 GHz, and that the success rate at 90 GHz may be far lower.

A recent pilot study at 90–100 GHz of a subset of sources detected in our 20 GHz survey shows that the ATCA can measure accurate continuum flux densities down to levels well below 100 mJy, and that the 8–20 GHz radio spectral index may be a good predictor of the observed flux density at 90 GHz (Sadler et al., in preparation). We therefore suggest that the 20 GHz source catalogues now being produced for the whole southern sky (Dec.  $\delta < 0^\circ$ ) in the AT20G survey will provide a more efficient way of identifying 90 GHz phase calibrators for ALMA than the currently proposed technique of extrapolation from radio surveys at 1–5 GHz.

### 8.1.4 ‘Flat-spectrum’ and ‘steep-spectrum’ populations

Earlier in this paper, we characterized the 20 GHz sources in terms of their position in the radio two-colour diagram shown in Fig. 7. This makes clear both the diversity of radio spectra seen in high-frequency sources and the difficulty of predicting high-frequency properties from low-frequency spectra. Studies of the cosmic evolution of radio sources, however, usually consider only two source populations – extended, steep-spectrum sources and compact, flat-spectrum sources. As discussed by Peacock (1985) these two populations can be understood physically, with the radio flux density being dominated by emission from extended radio lobes in steep-spectrum sources and a central compact core in flat-spectrum sources. In a sample selected at low frequency, the physically distinct optically thin diffuse emission has a distribution of spectral indices centred at  $-0.7$  and so the dividing line between ‘flat’ and ‘steep-spectrum’ sources is traditionally set at a spectral index of  $\alpha = -0.5$ . We note, however, that this division will be somewhat frequency dependent.

Radio-source samples selected at higher frequencies are increasingly dominated by flat-spectrum sources which are expected to be compact in nature. Even at 20 GHz, however, there is a minority population of objects which would be considered steep-spectrum using the normal convention of  $\alpha < -0.5$  at frequencies of 1–5 GHz. In terms of the overall properties of our sample, and as a guide for later comparison with other studies, it is therefore useful to note that our 20 GHz sample contains roughly 87 per cent ‘flat-spectrum’ and 13 per cent ‘steep-spectrum’ as defined by their low-frequency spectral index ( $\alpha_L$  in Table 5).

## 8.2 Polarization properties at 20 GHz

The high selection frequency of our survey makes it particularly useful for estimating the contribution of foreground radio sources to future studies of polarization fluctuations in the CMB radiation at 20 GHz and above.

Fig. 10 plots the fractional linear polarization measured at 20 GHz against the 20 GHz flux density, and shows that most sources selected at 20 GHz have low levels of linear polarization (typically 1–5 per cent). The median fractional polarization at 20 GHz is 2.3 per cent, but Fig. 10 suggests that there is a trend for fainter

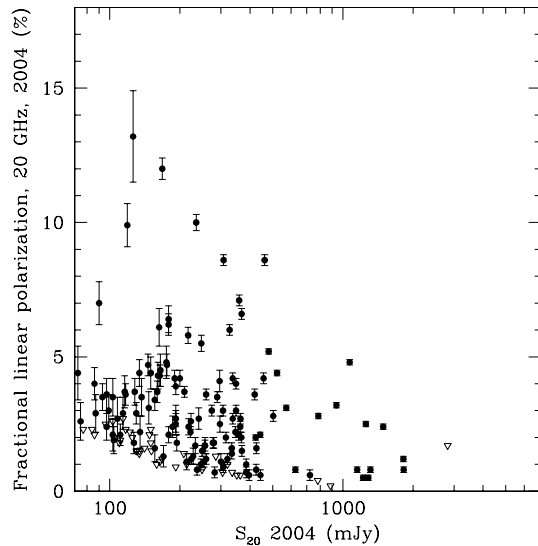


**Figure 10.** Fractional linear polarization at 20 GHz, measured in 2004. Open triangles show upper limits for sources where no polarized flux was detected.

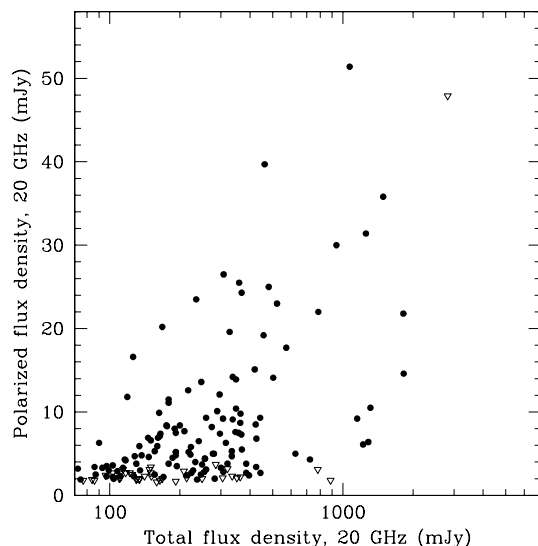


**Figure 11.** Total linearly polarized flux density at 20 GHz, plotted as a function of the total flux density. As in Fig. 10, open triangles show upper limits for sources where no polarized flux was detected. Note that although the weaker 20 GHz sources in our sample typically have higher fractional polarization, the strongest sources still dominate the source counts in polarized flux.

20 GHz sources to show higher levels of polarization (the median linear polarization is 2.7 per cent for sources with  $100 < S_{20} < 200$  mJy and 1.7 per cent for sources with  $S_{20} > 200$  mJy). A generalized Kendall's tau correlation test for censored data (Isobe et al. 1986) gives a value of 2.07, corresponding to a 3.9 per cent probability that the observed correlation is due to chance. Fig. 11 shows that the maximum polarized flux densities measured are 40–50 mJy, and so sources bright enough to calibrate CMB polarization experiments are rare.

The median fractional polarization of 2.3 per cent which we measure at 20 GHz for a flux-limited sample with  $S_{20} > 100$  mJy is very close to the median value of 2.2 per cent found by Mesa et al. (2002) for a flux-limited sample at 1.4 GHz with  $S_{1.4} > 80$  mJy.

Mesa et al. (2002) also observed a marginally significant trend for weaker sources to have a higher median polarization.

The similarity between the median polarizations observed at 1.4 and 20 GHz is somewhat surprising, since the 1.4 GHz sample is overwhelmingly dominated by steep-spectrum sources and the 20 GHz sample by flat-spectrum sources. Mesa et al. (2002) find a similar median polarization at 1.4 GHz for both steep- and flat-spectrum sources, and Tucci et al. (2004) argued that the mean level of polarization in flat-spectrum radio sources increases steadily with frequency. We might therefore have expected the median polarization in our sample to be higher than that observed at 1.4 GHz.

This does not appear to be the case, and a larger data set at 20 GHz is needed both to examine this issue in more detail and to compare the high-frequency polarization properties of the different spectral subclasses identified in Section 5 of this paper.

### 8.3 Variability of the source population at 20 GHz

In Section 6 of this paper we showed that the general level of variability of radio sources selected at 20 GHz sources appears to be low, with a median variability index of 6.9 per cent on a one-year time-scale (see Table 6). In the current sample, we find no significant correlation between the variability index of a source and its fractional polarization or radio spectral index. This is perhaps not surprising, since our sample is relatively small, and only a few of the sources are strongly variable.

The five most variable sources in our sample (with a variability index of 30 per cent or more) are J0507–6104, J0623–6436, J0820–6814, J1546–6837 and J1903–6749. Four of these are candidate QSOs of unknown redshift and one (J0623–6436) is a Seyfert galaxy at redshift  $z = 0.129$ . None of these radio sources appear to have been monitored previously, so nothing is known about their long-term behaviour.

Direct comparison of our results with previous studies is difficult, both because many of these studies are based on targeted rather than flux-limited samples, and because we have so far only analysed data from two measurements taken a year apart. The variability time-scales measured in this paper are all in the observed frame. The redshifts  $z$  of many of our sources are currently unknown, and we remind the reader that the observed variability time-scale will differ from the intrinsic value by a factor of  $(1 + z)$  so that longer monitoring is particularly important for the highest redshift sources.

Even at this stage, however, we can conclude that the general level of variability in sources selected at 20 GHz appears to be low on time-scales of 1–2 yr, and that source catalogues made at this frequency should therefore be robust on time-scales of at least a few years. Long-term monitoring studies of targeted sources by Valtaoja and co-workers (e.g. Valtaoja et al. 1988) show that even though many high-frequency sources have bursts of short-term variability, they are relatively quiescent for most of the time. This is entirely consistent with our results, and suggests that we should continue to monitor this source sample for a much longer period of time.

### 8.4 Conclusions

The pilot-study results presented here show that a sensitive 20 GHz radio continuum survey of the whole southern sky is feasible, and should produce a uniform source catalogue which is largely stable over time-scales of a few years. Such a survey should provide further insights into the nature of the high-frequency radio-source population, both in its own right and as a polarized foreground component in future CMB experiments like *Planck*.

**ACKNOWLEDGMENTS**

We acknowledge financial support from the Australian Research Council (ARC) through the award of a Federation Fellowship to RDE and an ARC Australian Professorial Fellowship to EMS. This research has made use of the NED which is operated by the Jet Propulsion Laboratory, California Institute of Technology, under contract with the National Aeronautics and Space Administration. We thank the referee, Prof. Ian Browne, for a number of helpful suggestions.

**REFERENCES**

- Akritas M. G., Bershadsky M. A., 1996, *ApJ*, 470, 706  
 Barvainis R., Lehar J., Birkinshaw M., Falcke H., Blundell K., 2005, *ApJ*, 618, 122  
 Bennett C. L. et al., 2003, *ApJ*, 583, 1  
 Bolton R. C. et al., 2004, *MNRAS*, 354, 485  
 Colless M. et al., 2001, *MNRAS*, 328, 1039  
 Conway J. E., Cornwell T. J., Wilkinson P. N., 1990, *MNRAS*, 246, 490  
 Fosbury R. A. E., Morganti R., Wilson W., Ekers R. D., di Serego Alighieri S., Tadhunter C. N., 1998, *MNRAS*, 296, 701  
 Hambly N. C. et al., 2001, *MNRAS*, 326, 1279  
 Harris A. I., Zmuidzinas J., 2001, *Rev. Sci. Instrum.*, 72, 1531  
 Hirabayashi H. et al., 2000, *PASJ*, 52, 997  
 Holdaway M., Carilli C., Laing R., 2004, ALMA Memo 493: Finding Fast Switching Calibrators for ALMA, <http://www.alma.nrao.edu/memos/>  
 Isobe T., Feigelson E. D., Nelson P. I., 1986, *ApJ*, 306, 490  
 Jackson C. A., Wall J. V., 1999, in Morganti R., Couch W. J., eds, *Looking Deep in the Southern Sky*. Springer-Verlag, Berlin, p. 11  
 Jackson C. A., Wall J. V., Shaver P. A., Kellermann K. I., Hook I. M., Hawkins M. R. S., 2002, *A&A*, 386, 97  
 Leahy P., 1989, VLA Scientific Memorandum No. 161, NRAO  
 Lo K. Y. et al., 2001, in J. Craig Wheeler, Hugo Martel, eds, *AIP Conf. Proc. Vol. 586, 20th Texas Symposium on Relativistic Astrophysics*. Am. Inst. Phys., New York, p. 172  
 Ma C. et al. 1998, *AJ*, 116, 516  
 Mauch T., Murphy T., Buttery H. J., Curran J., Hunstead R. W., Piestrzynski B., Robertson J. G., Sadler E. M., 2003, *MNRAS*, 342, 1117  
 Mesa D., Baccigalupi C., De Zotti G., Gregorini L., Mack K.-H., Vigotti M., Klein U., 2002, *A&A*, 396, 463  
 Owen F. N., Spangler S. R., Cotton W. D., 1980, *AJ*, 85, 3510  
 Peacock J. A., 1985, *MNRAS*, 217, 601  
 Peacock J. A., Gull S. F., 1981, *MNRAS*, 194, 331  
 Reynolds J. E., 1994, ATNF Memo AT/39.3/040, <http://www.atnf.csiro.au/observers/memos/d967831.pdf>  
 Ricci R. et al., 2004a, *MNRAS*, 354, 305  
 Ricci R., Prandoni I., Gruppioni C., Sault R. J., De Zotti G., 2004b, *A&A*, 415, 549  
 Sadler E. M. et al., 2002, *MNRAS*, 329, 227  
 Sault R. J., 2003, unpublished ATNF Memo, [http://www.narrabri.atnf.csiro.au/calibrators/data/1934-638/1934\\_12mm.pdf](http://www.narrabri.atnf.csiro.au/calibrators/data/1934-638/1934_12mm.pdf)  
 Sault R. J., Wieringa M. H., 1994, *A&AS*, 108, 585  
 Taylor A. C., Grainge K., Jones M. E., Pooley G. G., Saunders R. D. E., Waldram E. M., 2001, *MNRAS*, 327, L1  
 Tingay S. J., Jauncey D. L., King E. A., Tzioumis A. K., Lovell J. E. J., Edwards P. G., 2003, *PASJ*, 55, 351  
 Tornikoski M., Lahteenmaki A., Lainela M., Valtaoja E., 2002, *ApJ*, 579, 136  
 Tucci M., Martinez-Gonzalez E., Toffolatti L., Gonzalez-Nuevo J., De Zotti G., 2004, *MNRAS*, 349, 1267  
 Valtaoja E. et al., 1988, *A&A*, 203, 1

**APPENDIX A: NOTES ON INDIVIDUAL SOURCES IN TABLE 3****J0025–6028**

Double source with 23 arcsec separation, PA 159°.

**J0103–6439**

Wide double at 843 MHz, with 3.5 arcmin separation Only the core is seen at 20 GHz.

**J0121–6309**

Core plus 39 arcsec double, PA 14°.

**J0257–6112**

Core plus 10 arcsec jet, PA ~60°.

**J0425–6646**

This source was identified by Ricci et al. (2004a) with a magnitude 16.8 stellar object. The higher resolution radio image we obtained in 2004 makes it clear that the correct ID is a fainter stellar object slightly to the west.

**J0715–6829**

This source lies close to a bright (11th magnitude) foreground star, and no optical identification is possible from the SuperCOSMOS optical images.

**J0743–6726**

Core plus 12 arcsec jet, PA 117°.

**J1807–7012**

Double source with 27 arcsec separation, PA 114°, no core visible.

**J1822–6359**

Double source with 32 arcsec separation, PA 57°.

**J1824–6717**

Double source with 49 arcsec separation, PA 158°, no core visible.

**J2157–6941**

Core plus wide double source with 1.5 arcmin separation, PA 20°. Some flux may be missing at 18 and 20 GHz. This source has been studied in detail by Fosbury et al. (1998).

**J2306–6521**

Jackson et al. (2002) identify this source with a faint ( $B = 24$  mag) galaxy, for which they measure the quoted redshift of  $z = 0.470$ .

**J2358–6052 and J2350–6057**

Hotspots of the powerful radio galaxy PKS2356–61, as discussed by Ricci et al. (2004a).

This paper has been typeset from a  $\text{T}_{\text{E}}\text{X}/\text{L}_{\text{A}}\text{T}_{\text{E}}\text{X}$  file prepared by the author.